Final Summary Report

Period: January 15, 1965 - May 31, 1966

STUDY OF ELECTRON - PHONON INTERACTIONS IN III - V SEMICONDUCTORS

Dr. Joseph Martin - Principal Investigator

Contract NAS 3-20012

(Cost plus a Fixed Fee)

Control number DCN 1-5-23-01001-01(1F)

Research Institute for Advanced Studies
(RIAS - Martin Company)
1450 South Rolling Road
Baltimore, Maryland 21227

June 1966

Final Summary Report

Period: January 15, 1965 - May 31, 1966

STUDY OF ELECTRON - PHONON INTERACTIONS IN III - V SEMICONDUCTORS

Dr. Joseph Martin - Principal Investigator

Contract NAS 3-20012

(Cost plus a Fixed Fee)

Control number DCN 1-5-23-01001-01(1F)

Research Institute for Advanced Studies
(RIAS - Martin Company)
1450 South Rolling Road
Baltimore, Maryland 21227

June 1966

Acknowledgments

This report was prepared by the RIAS Division, Martin-Marietta Corporation under contract NAS 8-20012, "Study of Electron-Phonon Interaction in III-V Semiconductors" for the George C. Marshall Space Flight Center of the National Aeronautics and Space Administration. The work was administered under the technical direction of the Research Projects Laboratory, George C. Marshall Space Flight Center with Mr. William J. Robinson acting as project manager.

The author wishes to acknowledge the extensive help obtained from Dr. C. Y. Huang both in setting up the equipment and in discussion of the objectives and methods of the experiments. Dr. Louis Witten provided continuing encouragement and valuable aid in interpretation of experimental results. The technical assistance of Mr. E. Flanagan and Mr. G. H. Parr was essential.

3463

Abstract

The study of electron-phonon interactions in semiconductors was initiated with an evaluation of several known transducer techniques for generating microwave phonons. Piezoelectric excitation was chosen and some tourmaline and quartz crystals were examined for use as transducers at 9.3 Gc/sec. A large variability was observed from one crystal to another in transduction efficiency at 4.2°K. The temperature dependence of microwave phonon attenuation was measured in quartz and in green and black tourmaline. The quartz measurements covered a very wide dynamic range and were very consistent from one crystal to another. These data were in very good agreement with measurements by other investigators over limited portions of this dynamic range. The temperature dependence obtained was compared with several published theories, none of which was completely adequate. The attenuation in tourmaline was quite different in its temperature dependence from quartz and other crystals. It exhibited a very fast change of slope with increase in temperature but could not be compared to existing theories since necessary auxiliary data is not available for tourmaline. Quartz crystals were used as transducers to generate microwave phonons in InSb semiconductor crystals. Dislocation damping was found to be a strong source of phonon attenuation in boat-grown InSb crystals. Czochralski grown crystals had a much lower dislocation density. A decrease in attenuation with temperature increase was observed in InSb between 4.2°K and 15°K. Also, a small frequency shift of about + 2 Mc/sec was observed in phonons which traversed the InSb crystal. The above effects were measured consistently but the consistency was only qualitative. A further investigation of these effects is being pursued.

Table of Contents

A. Introduction

Phonon interactions in solids have attracted a great deal of research effort since such interactions can serve as useful probes, often quite different from electromagnetic interactions, into the structure and properties of the solids. Traditionally thermal conductivity and diffusion, heat capacity, and, spin lattice relaxation times have been used to study the behavior of phonons in solids. In these experiments the phonons studied consisted of the thermal distribution of lattice vibrations. More recently, slow neutron diffraction studies have been useful in studying thermal phonon behavior.[1]

In recent years, the techniques for generating coherent beams of phonons with frequencies approaching thermal distributions in the liquid Helium range have been developed[2,3] and used to study phonon interactions in solids. The interactions of these phonons, with charge carriers, thermal phonons, crystal impurities, dislocations and spin systems are subjects of fruitful study.

The prime object of the present contract is an experimental study of the interaction of microwave phonons with conduction electrons in semiconductors. A considerable amount of work has been done both experimentally[4-6] and theoretically[7-9] on the interaction of megacycle phonons in metals. In recent years many workers[10-17] have investigated both attenuation and gain in semiconductors, particularly CdS. In CdS

the electron-phonon interaction is principally through the piezoelectric effect, whereas in non-piezoelectric semiconductors the interaction is principally through deformation potential coupling.

Calculations made by Spector[15] suggest that the electron-phonon interaction in non-piezoelectric semiconductors increases linearly with frequency in the high frequency region. This strong interaction would produce a high attenuation of a phonon wave unless the electrons in the solid are moving in the direction of the ultrasonic wave with a velocity exceeding that of the phonons. In this case the attenuation would be negative giving a gain in phonon energy. The other phonon interactions such as scattering from thermal phonons, impurity scattering, and crystal defect scattering are also sources of attenuation. Thus even though a high attenuation might be measured in a material, the corresponding gain which should occur when the electron drift velocity exceeds the sonic velocity might not be as high as expected on the basis of the electron-phonon interaction alone.

The present study was directed primarily at the experimental investigation of electron-phonon interactions in III-V semiconductors at 9.3 Gc/sec. In the course of the research it was considered worthwhile to study in some detail the characteristics of the transducers being used to generate acoustic waves in the semiconductors. Thus the temperature variation of 9.3 Gc/sec phonon attenuation in quartz and tourmaline crystals was measured. Conditions governing the propagation of these phonons in a high mobility III-V semiconductor, InSb, were studied experimentally.

B. Transducers

In the beginning of the program it was decided to use transducer techniques which are already known rather than to work on the development of new techniques since there are laboratories working on such developments. Two proven transducer techniques were set up in our laboratory to test their applicability to our program of investigation of electron-phonon interactions. These two techniques for generation of microwave phonons are 1) piezoelectric excitation of a piezoelectric crystal bonded to the crystal under study[2], and 2) magnetostrictive excitation in a thin ferromagnetic film[3, 17].

The magnetostrictive excitation method has the advantage over the piezoelectric method of not being very dependent on temperature and of being able to produce both transverse modes and the compressional mode in the same film. Furthermore a reproducible bond can be obtained in evaporating the film onto a well-cleaned polished surface. The piezoelectric method on the other hand is independent of magnetic field, and therefore the magnetic field can be treated as an independent parameter. It was decided therefore to make the initial studies with the piezoelectric method using longitudinal waves in order to simplify the analysis of effects in the semiconductor.

1. Piezoelectric excitation

Two piezoelectric materials were examined for use in this program, quartz and tourmaline. Quartz has been used extensively at

microwave frequencies to study the phonon-phonon interactions in itself[2,18]. Tourmaline has not been examined before at these frequencies. The studies performed (on quartz and tourmaline) under the present contract involved careful measurements of the temperature dependence of phonon attenuation as well as of the variability of efficiency of the crystals.

The microwave equipment used for these measurements is shown in block diagram in Figure 1. Most of this equipment can be seen in the photograph of the working setup shown in Figure 2. The measurements were all made in the liquid Helium cryostat seen in Figure 2. Microwave pulses 0.6 μsec wide at a repetition rate of 40 pulses/sec and a peak power of 5 kw were obtained from a Paradynamics Model X890A microwave signal source. The frequency was held at 9.3 Gc/sec for most of the measurements although it was actually variable from 8.8 to 9.4 Gc/sec. These pulses were attenuated by at least 20 db before entering the resonant reentrant cavity holding the piezoelectric crystal. The average power pumped into the cavity was therefore < 120 mw.

A 20 db isolation circulator (Rantec model CX-425) was used to route the microwave power into the cavity and to route the cavity output signal to the mixer-detector. A microwave diode switch (Arra model X110) was added to the receiver line to reduce the amplifier saturation caused by the power pulse leakage in the circulator.

The reentrant cavity was fabricated out of brass and plated inside with silver to increase the Q. A view of the cavity before final

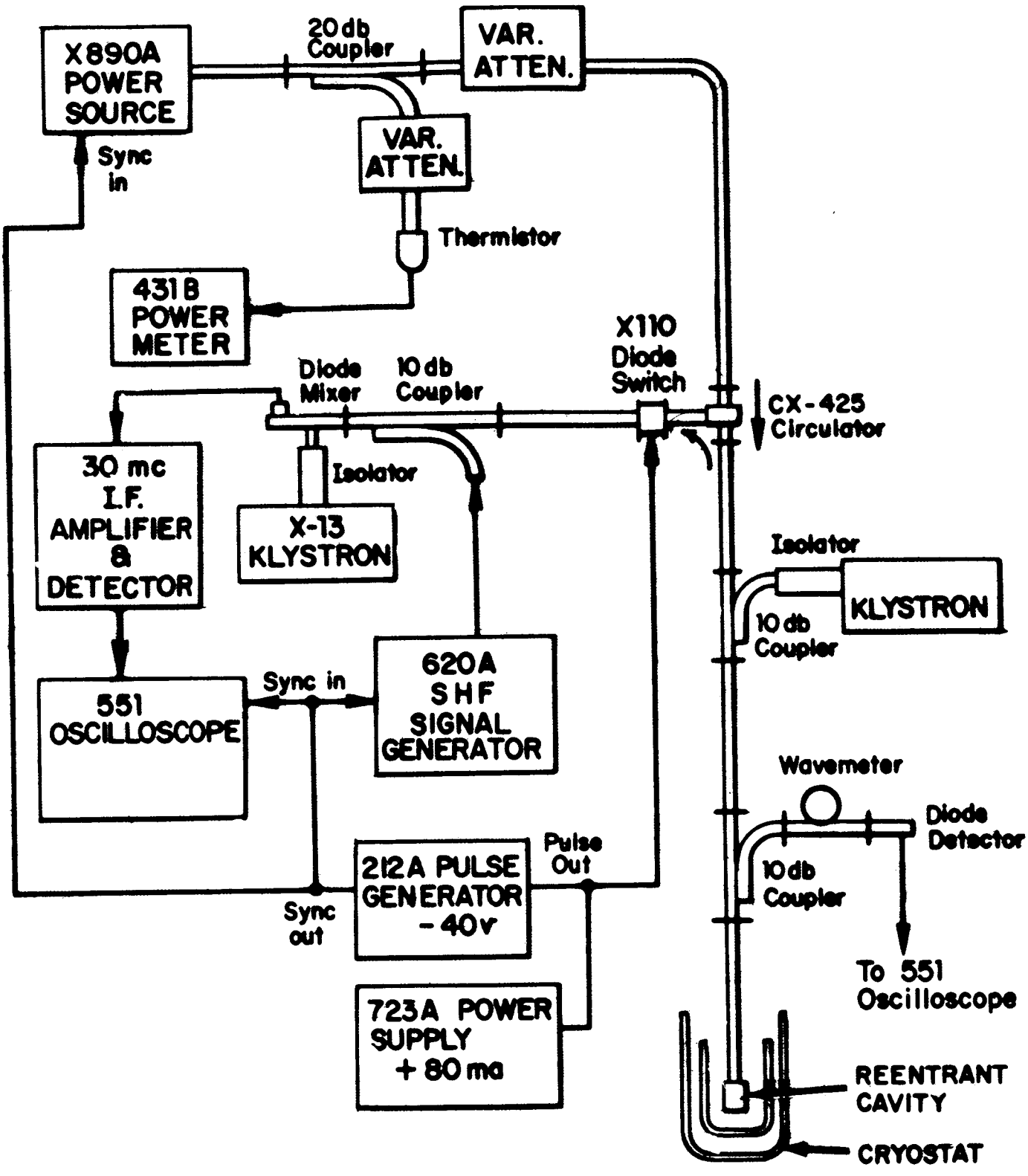

Fig. 1 Microwave Circuitry for Acoustic Attenuation

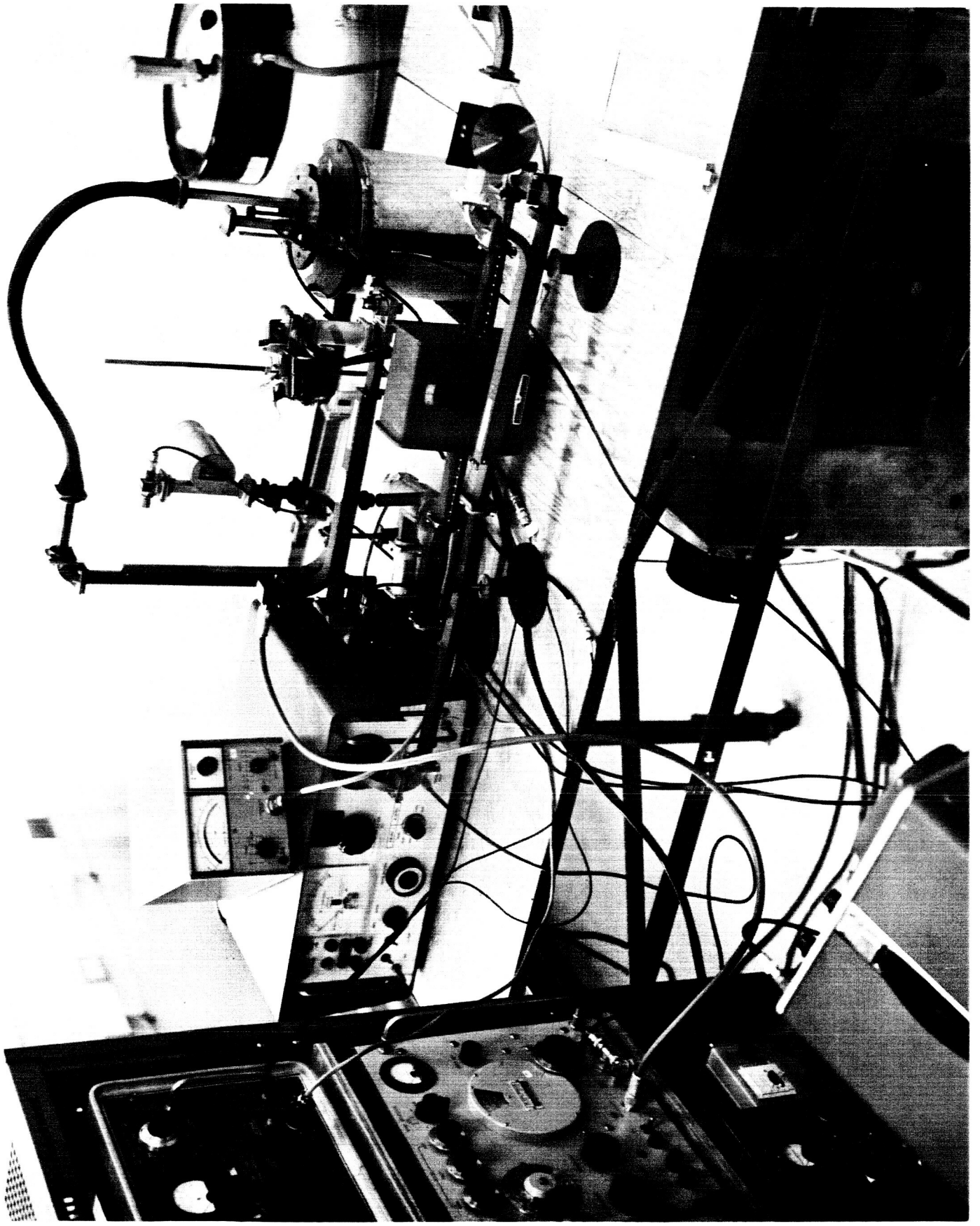

Fig. 2 - Microwave phonon generation and detection equipment.

assembly is shown in Figure 3 along with a photo of the cavity assembled onto the waveguide with a quartz crystal plus InSb crystal in place. The resonant frequency was adjusted at room temperature by adjusting the depth of insertion of the crystal into the cavity. This frequency was measured using a frequency modulated klystron and a calibrated wavemeter cavity. The resonant frequency usually shifted down about 25 mc when the temperature was lowered to $4.2^{\circ}K$.

The microwave electric field inside the cavity is a maximum at the end of the center post where the piezoelectric rod is inserted. Microwave power is converted to acoustic power at the end of the crystal inside the cavity by the piezoelectric effect. The acoustic wave thus generated propagates down to the other end of the crystal. In the tests on the transducer crystals there was nothing attached to this other end, but in the semiconductor studies the semiconductor was bonded to the other end. The acoustic wave was partially reflected and partially transmitted at the bonded interface. Thus the reflected acoustic pulses both from the interface and from the other end of the semiconductor arrived back at the generating surface in the cavity. Upon arriving at this surface, part of the acoustic power was converted back piezoelectrically to microwave power where it was observed by the detector system. However, most of the acoustic power was reflected back again such that multiple acoustic reflections occurred in the crystals. In all the experiments made, the time duration of the microwave pulse (0.6 μsec) was shorter than the time of propagation of the acoustic wave through the crystal.

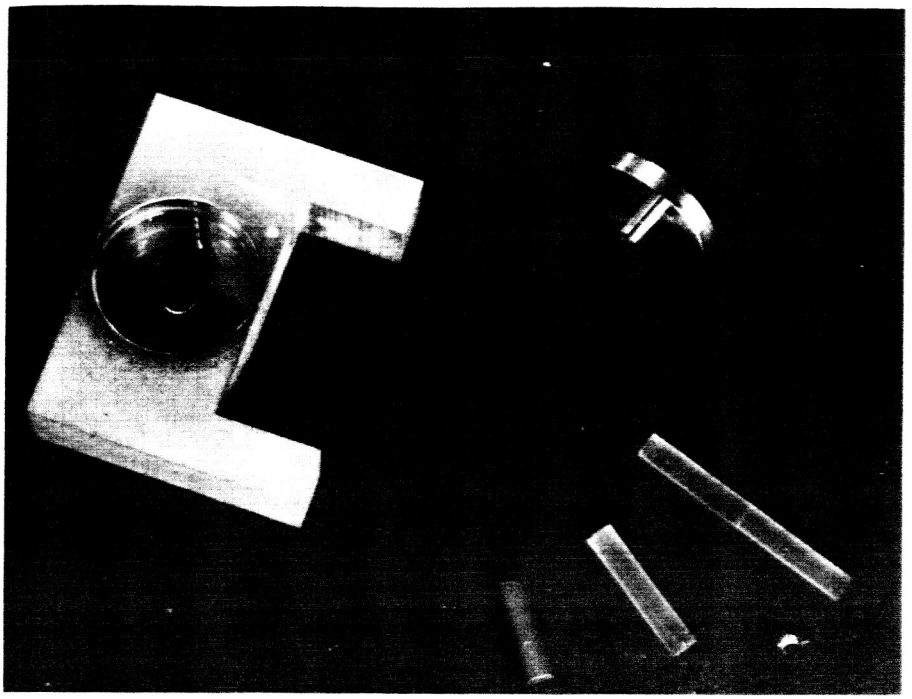

Figure 3a View of reentrant cavity shown before final assembly with quartz and InSb crystal rods

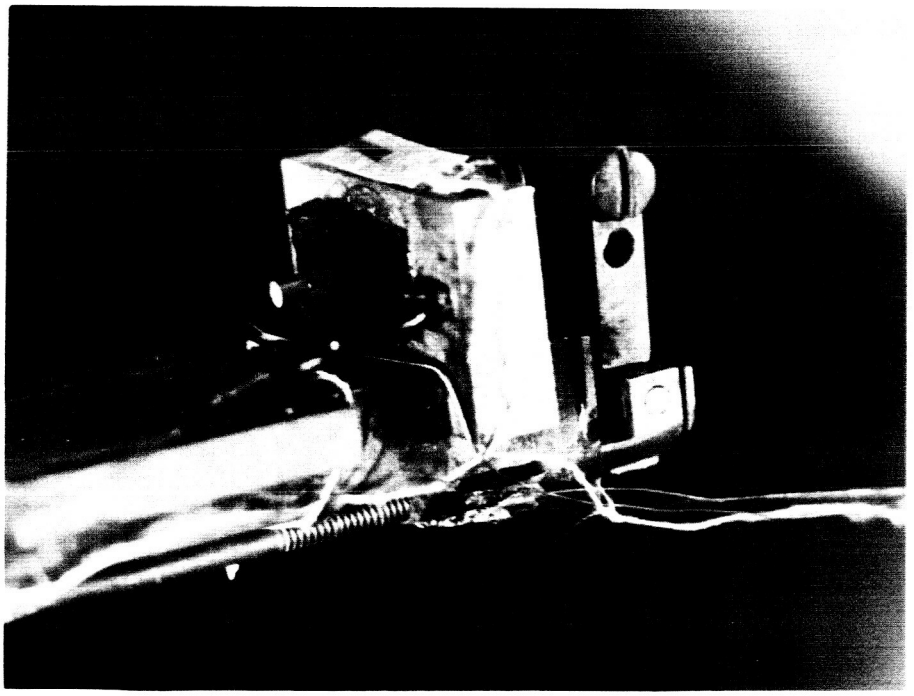

Figure 3b Cavity assembled onto waveguide with InSb bonded to quartz in place.

Thus the acoustic echoes were observable as distinct pulses in the receiver.

In order to measure the attenuations involved in these experiments a calibrated microwave signal generator was used as a comparator. (Hewlett Packard SHF Signal Generator Model 620A). The pulses from this signal generator were adjusted to the same width and frequency as the X890A pulses. These were fed into the same superheterodyne receiver system as were the reflected pulses from the crystals. A Varian X-13 klystron was used as local oscillator to obtain 30 mc IF signals which were then amplified and detected for comparison on the oscilloscope.

The 620A signal generator was also used to calibrate the attenuation of all parts of the microwave circuitry used in these experiments. The average power output of the X890A signal source was measured and monitored by a calibrated thermister power meter (Hewlett Packard X486A and 431B).

2. Magnetostrictive excitation

Although this method was not used for the measurements with the semiconductors during the first year of the program the equipment was set up for its use during subsequent phases of the program. In this case it is the microwave magnetic field which is necessary for the excitation so that the strong electric field of the reentrant cavity is not necessary. A rectangular TE_{102} cavity was used with the film placed in the central

magnetic field of the cavity. The microwave equipment was the same as that used for the piezoelectric excitation method. A nickel film of approximately 3000 Å thickness was evaporated onto an AC cut quartz rod and tested in the rectangular cavity. The oscilloscope photos in Figure 4 show the acoustic echoes obtained for three different magnetic field configurations. Both transverse modes are visible in Figure 4a where the DC magnetic field (H_{dc}) of 1.6 kgauss in the plane of the film was perpendicular to the microwave magnetic field (H_{ac}). Only the fast transverse mode can be seen in Figure 4b with H_{dc} = 2.1 kgauss parallel to H_{ac}. When H_{dc} was reduced from 2.1 kgauss to 0.4 kgauss while still parallel to H_{ac} the longitudinal phonons generated at the magnetic "stripe" domain walls became visible.[19] They are not very large however because the AC cut quartz crystal suppresses longitudinal waves.

3. Power loss tests in tourmaline and quartz

a. Tourmaline

It is known[2] that the attenuation of microwave phonons in quartz is quite small below 20°K but rises very rapidly above this temperature. The attenuation in quartz will be discussed further in section B-4. In order to determine whether some other piezoelectric crystal could effectively serve as a transducer at temperatures above the usable limit for quartz (about 35°K), tests were made with tourmaline crystals.

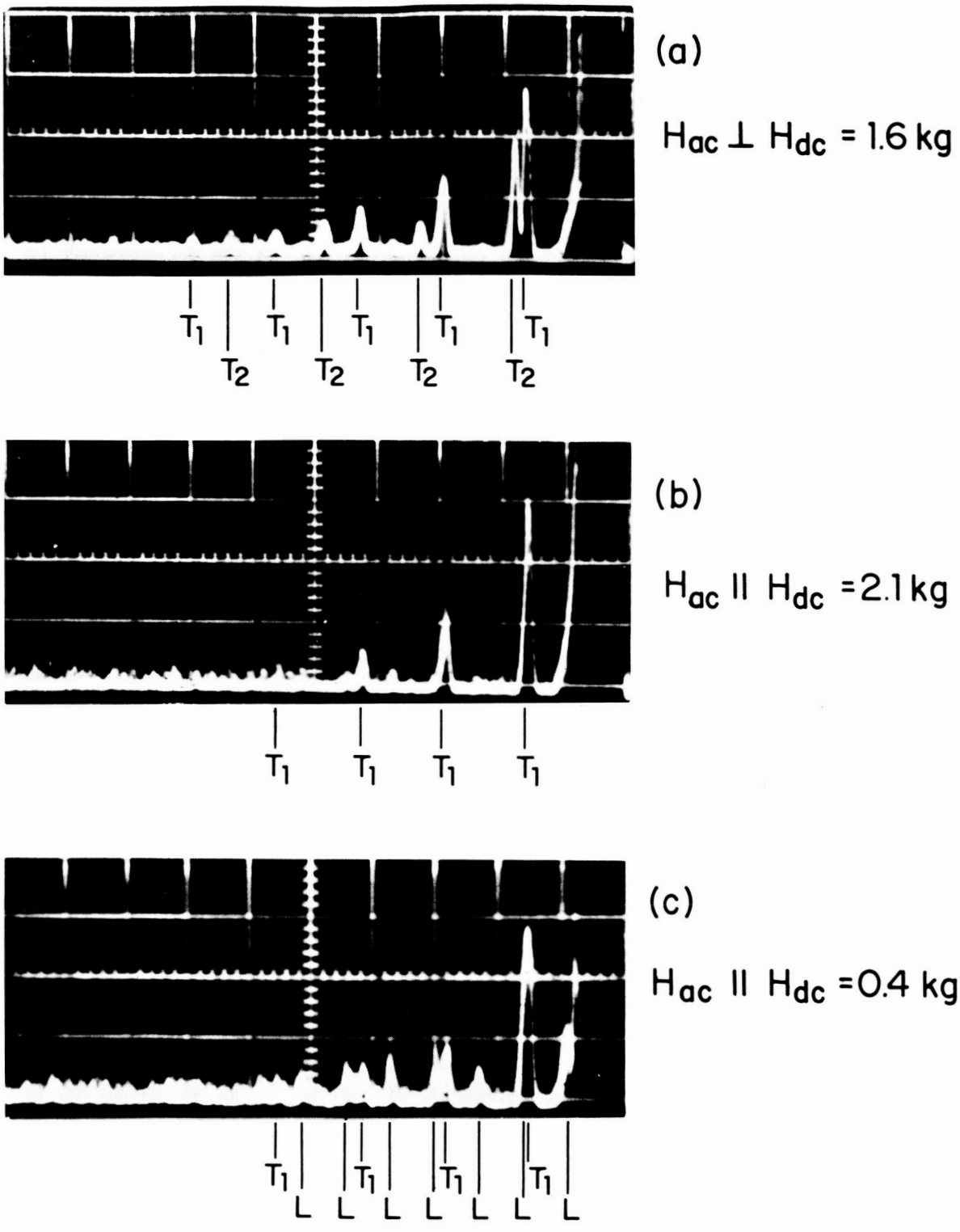

Figure 4 Acoustic echoes in AC cut quartz generated by magnetostrictive excitation of a thin film of nickel (T_1 = fast transverse wave, T_2 = slow transverse wave, L = longitudinal wave).

A batch of 6 black tourmaline rods and another batch of 6 green tourmaline rods were obtained from the Valpey Crystal corporation with following specifications. Length = 0.500" ± 0.001", diameter = 0.118" ± 0.001", rod axis parallel to the crystallographic z-axis to within 2 min., and end faces polished flat and parallel to 500 Å.

The net power loss involved in the acoustic transition (from microwave signal into the cavity back again to a microwave signal out of the cavity) for the first echo was measured at 4.2°K for all but two of these rods: The results are given in Table I

Table I

Measured net power loss involved in the acoustic transition at 9.3 Gc/sec for the first echo in green and black tourmaline rods at 4.2°K.

Rod No.	Green	Black
1	90 db	105 db
2	> 109 db (crack)	83 db
3	70 db	104 db
4	----- (crack)	105 db
5	105 db (crack)	92 db
6	------ (crack)	109 db

The measurements were made by comparison with the signal generator pulses. The numbers were obtained by calculating the input power from the thermister

power meter measurements and using all the previously calibrated attenuations in the microwave system. Four of the green tourmaline rods were found to have internal cracks. Two of these were tested and found to have a very high attenuation. The other two were not tested. Since the black tourmaline crystals are completely opaque it was not possible to tell if there were any internal cracks in these. Although no crack was observed in green tourmaline #1 before testing, there was a small one observable after the test at $4.2^{\circ}K$. This is consistent with the rather poor loss figure of 90 db. The power loss of 70 db observed for green rod #3 compares very favorably with quartz, as will be seen in Table II.

b. Quartz

A batch of 10 quartz crystal rods were obtained from Industrial Optics Company, Bloomfield, New Jersey both for temperature dependence of attenuation in quartz and for use as transducers for the semiconductor studies. The specifications for these rods were the same as for the tourmaline rods except that the parallelism was to 200 Å and the rod was oriented along the x-axis. Each crystal was tested at $4.2^{\circ}K$ in the same way as the tourmaline rods.

The net power loss involved in the acoustic transition in both directions was measured for these rods as for Tourmaline and the results are shown in Table II.

Table II

Measured net power loss involved in the acoustic transition at 9.3 Gc/sec for the first echo in natural quartz rods at $4.2^{\circ}K$

Rod No.	1	2	3	4	5	6	7	8	9	10
Net Loss (db)	69	74	81	71	86	71	69	76	68	69

Besides the variation in net loss from one crystal to another, there was a considerable variation in the echo patterns observed. Furthermore, the echo pattern from any one crystal was not reproducible from one day to another. Figure 5 shows a case history for Quartz rod #9 as the rod was cycled repeatedly to $4.2^{\circ}K$. The crystal was cycled from room temperature between the first and the second and between the 3rd and 4th cycles. It was cycled from approximately $150^{\circ}K$ the other times. It is quite apparent from Figure 5 that the echoes deteriorated considerably with each thermal cycle. In the first cycle 247 echoes were visible while only 15 were visible in the last cycle. Not only is there a deterioration in the number of echoes but the echo pattern shows a significant change in the location of the maxima and minima and their relative amplitudes. In all the thermal cycles, the warming was slow (~several hours) and the cooling was fast (~several minutes).

The echo patterns for all the crystals, typified by Figure 5 for crystal #9, exhibited the complicated structure of maxima and minima

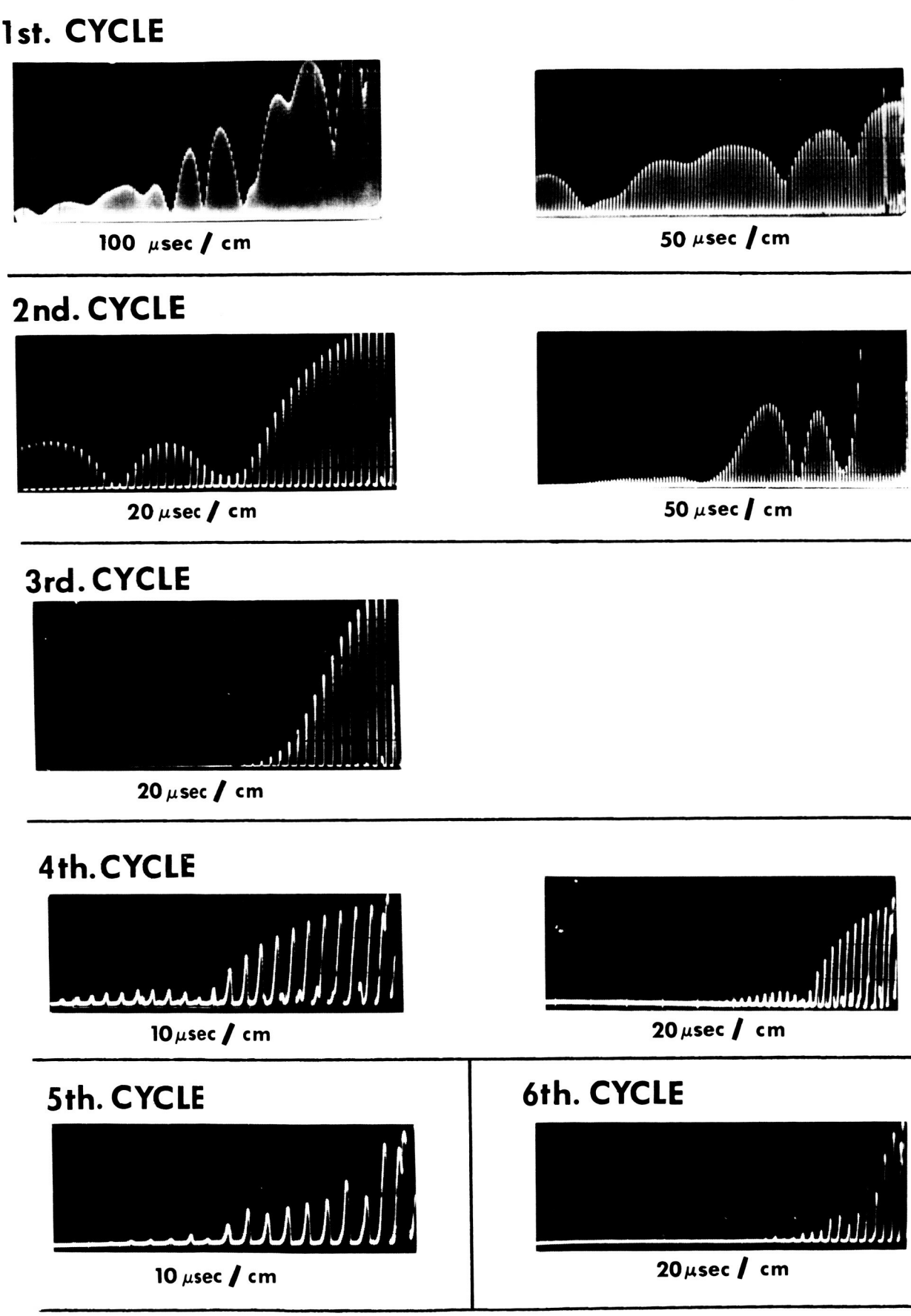

Fig. 5 **Degradation of 9.3 gc acoustic echoes in quartz with thermal cycling to 4.2° K.**

usually associated with acoustic measurements at these frequencies.[2] The interference pattern is no doubt partly due to the lack of exact parallelism of the end faces. However, if this were the only cause then the interference pattern would have a well defined period with an exponential decay envelope for the maxima. The limited flatness of the faces contributes to the evident irregularity in the interference pattern. It is very likely that structural strains and nonuniformities contribute also to this effect. Evidently some structural changes occur during thermal cycling as seen by the large changes in echo pattern observed in Figure 5. It is possible that all the changes are due to changing of strains in the crystal which reduces the parallelism of the end faces. The understanding of the nature of these interference patterns is quite incomplete as has been pointed out by Tepley.[6]

4. Temperature dependence of attenuation in tourmaline and quartz

The temperature of the crystals in these experiments was measured with the use of a doped germanium resistance thermometer Model CG3, obtained from Radiation Research Corporation, Westbury, New York. This thermometer was calibrated against a AU-Co vs Cu thermocouple. The 0.005" diameter Au-Co wire (obtained from Sigmund Cohn Corp., Mt. Vernon, N. Y.) was of the composition 2.11 Atomic per cent Cobalt as prescribed by Powell and Bunch.[20] Two thermocouple junctions were immersed in liquid Helium and liquid Nitrogen respectively and the EMF measured. The value obtained agreed

exactly with the EMF difference for these temperatures as published by Powell and Bunch.[20] Thus their calibration data was used as the calibration for the thermocouple.

During the attenuation measurements the Ge thermometer was inserted in a hole in the brass block of the resonant cavity (see Figure 3b) while a heater resistor was attached to the bottom of the cavity. The temperature was adjusted by adjusting the current in the heater and the position of the cavity above the liquid helium level. Equilibrium temperatures were thus obtained with an absolute accuracy of about $1^{\circ}K$ and a relative accuracy of $0.1^{\circ}K$. The limitation in the absolute accuracy is due to the lack of certainty of the temperature of the crystal itself as compared to the temperature at the thermometer. The calibration of the CG3 thermometer is shown in Figure 6.

a. Tourmaline

Green rod number 3 and black rod number 2 were used in making the measurements of temperature variation of the attenuation. These were respectively the best of their batches. Typical echo patterns for a green and a black tourmaline rod at $4.2^{\circ}K$ are shown in Figure 7.

The attenuation as a function of temperature was obtained by measuring the attenuation relative to that at $4.2^{\circ}K$. The results for green tourmaline #3 and black tourmaline #2 are shown in Figure 8. It is

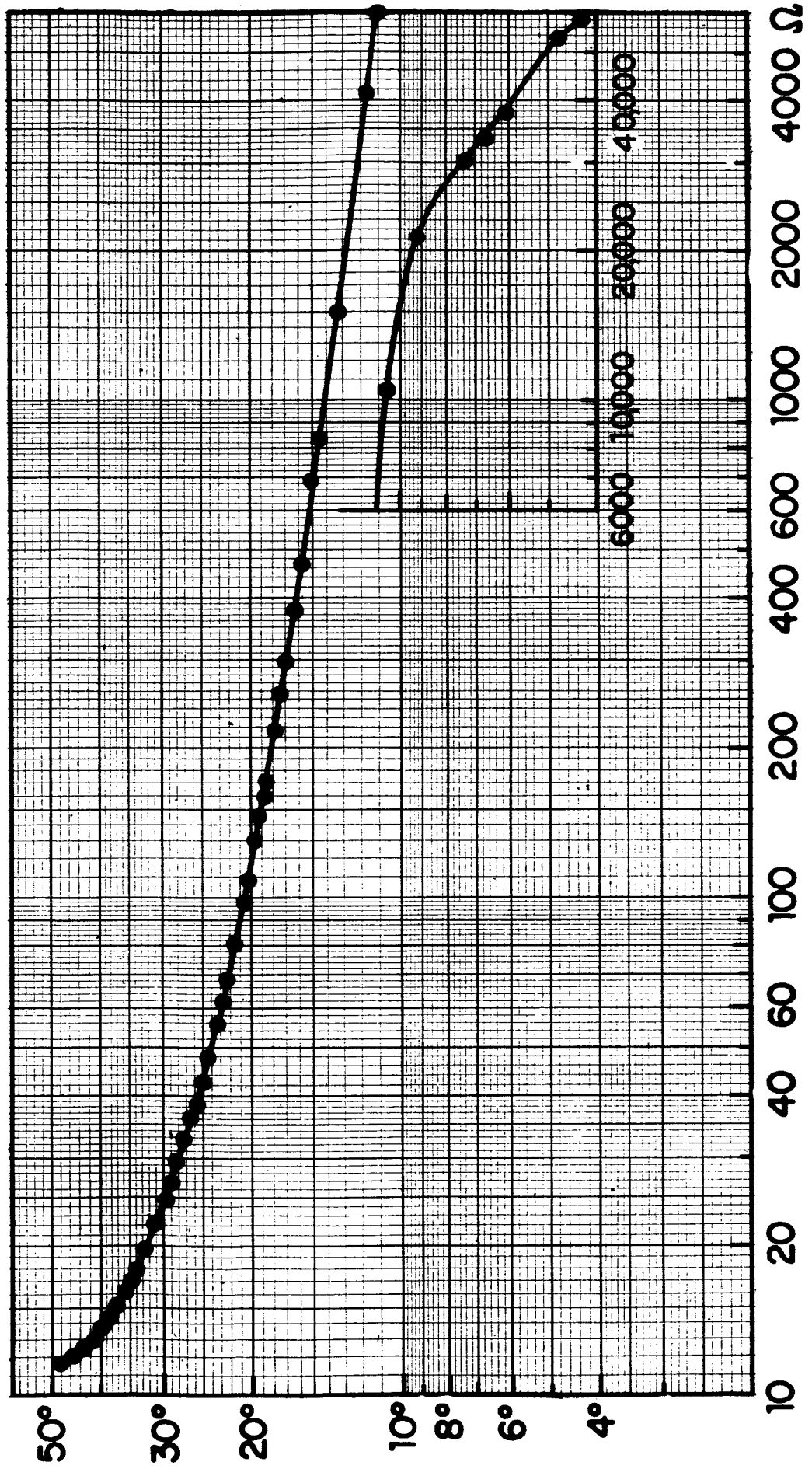

Fig. 6 Calibration of CG3 Ge Resistance thermometer in ^{o}K.

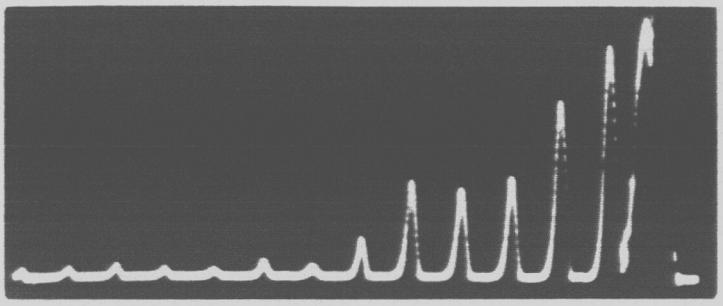

Green Tourmaline #3

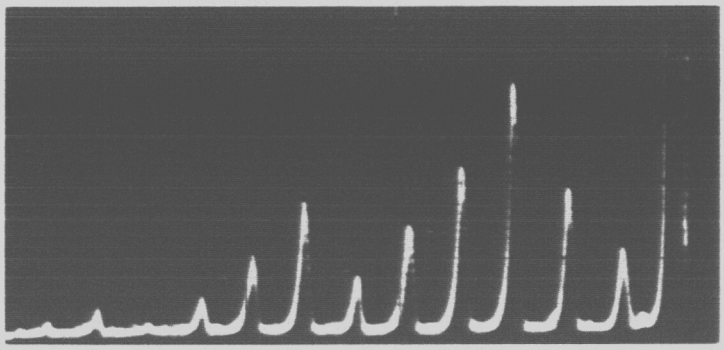

Black Tourmaline #5

Figure 7 Typical echo patterns for 9.3 Gc/sec phonons in tourmaline at 4.2°K

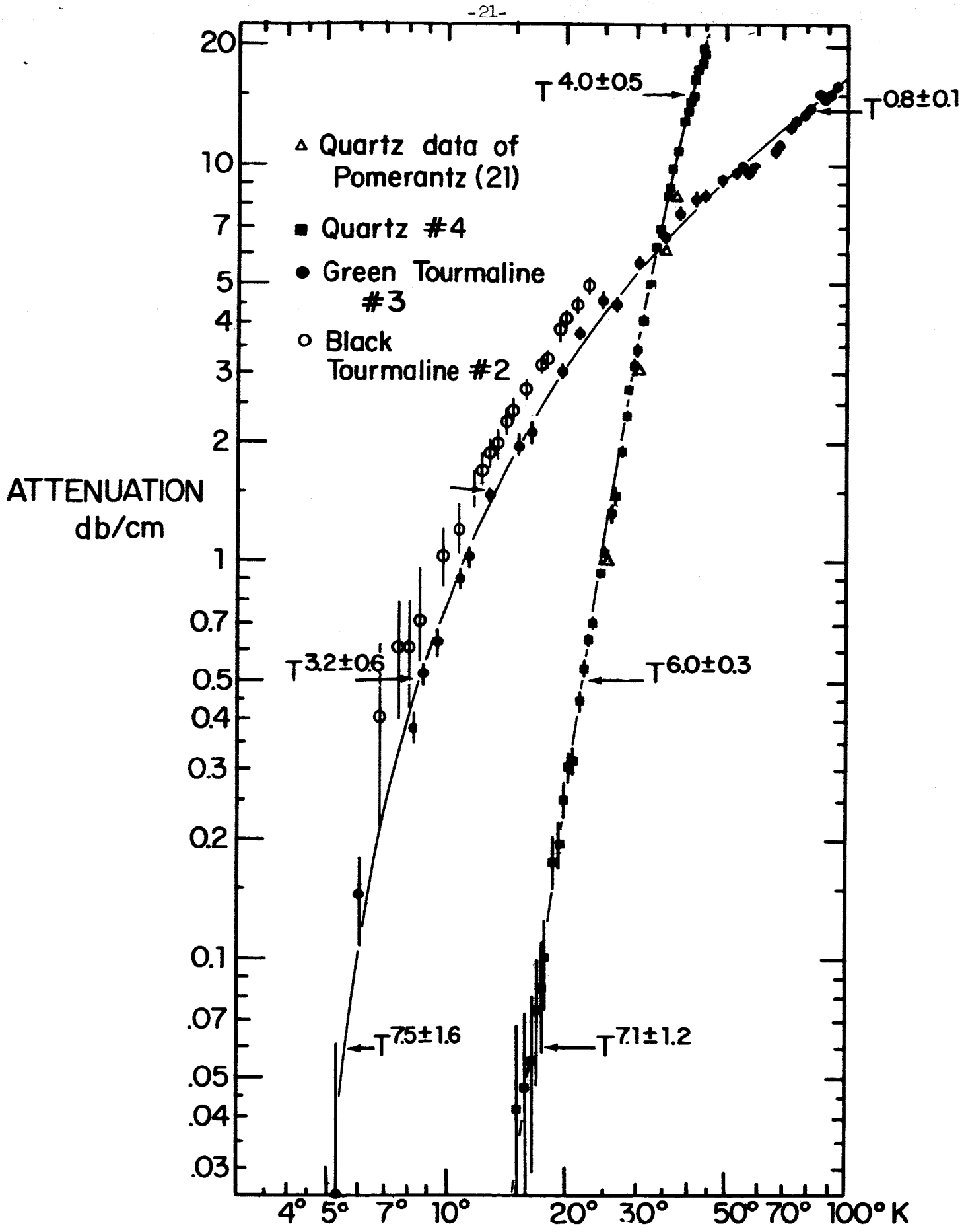

Fig. 8 Relative accustic attenuation in tourmaline and quartz at 9.3 Gc/sec

evident that the temperature dependence of the two are very similar, even though the net power losses for the first echo given in Table I differ by 13 db. Several echoes were used in determining the attenuation. At the higher temperatures, only the first echo was visible and so only this echo was used. At the lower temperatures, however, since more echoes were present, they were used to obtain more accurate determinations of the attenuation per cm. The temperature dependence of the tourmaline will be discussed in more detail in comparison with the temperature dependence of quartz.

b. Quartz

Measurements of the temperature dependence of 9.3 Gc/sec acoustic attenuation were made on Quartz rods #4 and #9. Such measurements have been made by others[21,22] over a limited dynamic range so that these data served as a check of the experimental procedure against the results of other investigators. Our measurements considerably expand the dynamic range of the measurements compared with the previous ones. Figures 8 and 9 show the results attained for quartz along with a comparison with the data of Pomerantz[21] and Nava et al[22] at 9 Gc/sec and with our results for green tourmaline. It is quite evident that although the slopes for quartz and tourmaline are approximately the same at lower temperatures the slopes differ markedly at the higher temperatures. It is evident also that green tourmaline can be useful as a transducer up to a much higher temperature than quartz.

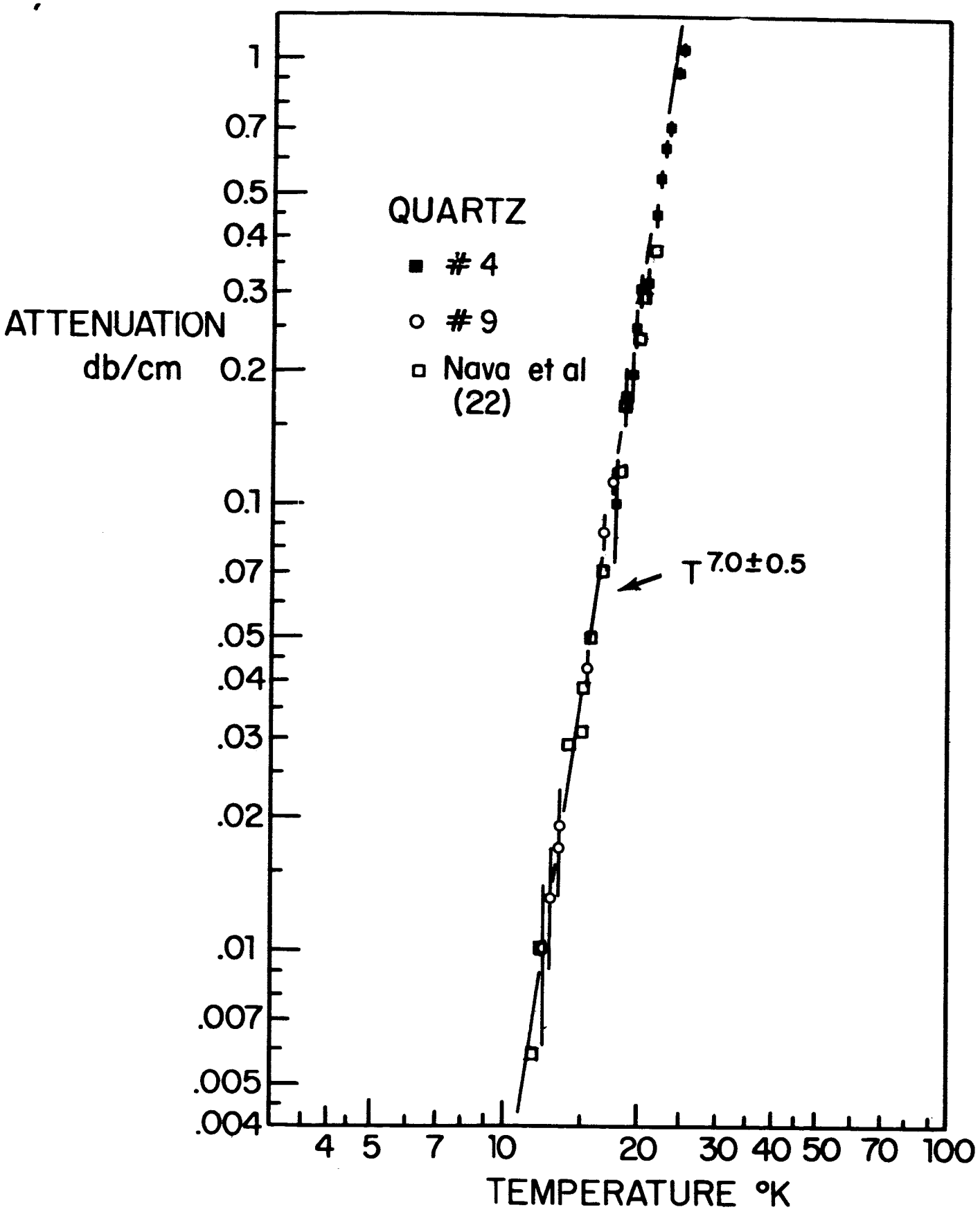

Fig. 9 Relative acoustic attenuation in quartz at 9.3 Gc/sec

The echo pattern for quartz crystal #4 allowed no echo beyond the fifteenth to be suitable for attenuation measurements. Thus this echo was followed up to 24.9°K after which it became too small to measure. The sixth echo was followed up to 28.6°K, the third up to 33.8°K, the second up to 36.9°K and the first up to 44.1°K. The accuracy of the data for this crystal at the lower temperatures in Figure 8 was limited by the $\pm$ 1 db accuracy in making the signal comparison measurement. Thus crystal #9, which exhibited the largest number of echoes (247) in its initial test, was chosen to extend the measurements so that the attenuation of one of the later echoes could be followed. This would yield a much higher db/cm accuracy than was possible with the fifteenth echo in crystal #4. (The 200th echo e.g. would represent a 508 cm acoustic path so that a very small attenuation/cm would still represent a rather large absolute attenuation and could be measured with good accuracy.)

When crystal #9 was cooled a second time (after the initial test) in order to make temperature variation measurements using the 200th echo, it was found that all the echoes beyond the 104th had disappeared as we noted in Figure 5. The 90th echo was therefore used to obtain the data shown for crystal #9 in Figure 9. It is evident from this data that the temperature dependent part of the attenuation is rather independent of the particular crystal.

c. Discussion of quartz and tourmaline results

Pomerantz[21] has made some measurements of microwave phonon attenuation at 9.0 Gc/sec using magnetostrictive excitation of Permalloy

films for a number of different crystals. Quartz was included among these. His published results for longitudinal phonons showed a linear relationship for all the crystals on the log attenuation vs log temperature plot. His data, however, covered only the attenuation range from 1 db/cm to 10 db/cm. Our measurements for quartz and tourmaline on the other hand show a distinctly non-linear relationship for both materials over the dynamic range measured (0.01 db/cm to 20 db/cm). Pomerantz thus found each crystal to have a temperature dependence of T^n with n varying somewhat from one crystal to another. As can be seen from Figure 8, his data are consistent with ours over the range which they cover, although we can definitely see a change of slope in our data which is not obvious in his. He obtained also an empirical prescription relating the Debye temperature of the material to the acoustic attenuation. Thus the temperature at which the attenuation is 3 db/cm corresponds to 0.1 θ_D. This would yield for our measurement $\theta_D = 190^\circ K$ for tourmaline and $\theta_D = 290^\circ K$ for quartz. The values given by Anderson[23] are $769^\circ K$ and $585^\circ K$ for tourmaline and quartz respectively. This is in sharp disagreement with the Pomerantz prescription although Lord and Morrow[24] use a value of $254^\circ K$ for the Debye temperature of quartz.

Nava and co-workers[22], on the other hand, measured the attenuation of longitudinal waves in x-cut quartz at 9.0 Gc/sec covering the range between 0.01 db/cm and 3 db/cm. The agreement with our measurements in this range is excellent exhibiting also a T^7 dependence. Thus the T^4 dependence quoted by Pomerantz[21] and the T^7 seen by Nava et al[22] are both consistent with our data whose dynamic range covers both these experiments.

At a frequency of 1 Gc/sec, de Klerk[25] measured the attenuation in Al_2O_3 over a wide dynamic range and observed a change of slope also. In his work it appears as though the slope is uniform over a certain range and then breaks sharply, while this is not true in our measurements -- the change seemed more gradual. His data for longitudinal phonons gives a T^9 dependence at lower temperatures with an abrupt change to T^4 at higher temperatures. For transverse phonons he observed such a change from T^7 to T^4 for fast shear waves, but he observed a constant T^4 dependence for slow shear waves.

The change of slope in our tourmaline measurements is considerably more striking than in the quartz. Tourmaline shows a change in T^n from $n = 7.5 \pm 1.6$ to $n = 0.8 \pm 0.1$ while quartz changes from $n = 7.0 \pm 0.5$ to $n = 4.0 \pm 0.5$. The fast change of slope observed in Tourmaline appears similar to that seen by other investigators[18,26] at lower frequencies in materials such as quartz, Al_3O_3 and MgO. This appears to be the first time that the flattening out of the attenuation curve has been measured at a frequency above 3 Gc/sec.

Landau and Rumer[27] worked out a quantum mechanical theory for phonon-phonon scattering involving three-phonon processes valid when $\omega\tau \gg 1$ (τ is the thermal relaxation time calculated[28] from $\kappa = 1/3\ C_v c^2 \tau$, κ = thermal conductivity, C_v = specific heat, c = average sound velocity). For Quartz at $40^\circ K$, $\tau = 2.2 \times 10^{-10}$ sec. Thus at 9.3 Gc/sec and $40^\circ K$, $\omega\tau \sim 13$. It is even larger at lower temperatures and so the theory would be expected to apply. Thermal conductivity measurements on tourmaline are not available so this estimate cannot be

made for tourmaline. The theory predicts a T^4 dependence for the attenuation which agrees well with our quartz measurements above $35^{\circ}K$.

However, Landau and Rumer[27] indicate that their theory should apply only to transverse acoustic phonons and not to compressional phonons. This is because the conservation of energy and momentum in a three-phonon process requires that all three phonons cannot have the same propagation velocity unless they are exactly co-linear. Assuming that thermal phonons are only longitudinal, the longitudinal acoustic phonons could not satisfy this condition with a finite interaction solid angle. On the other hand Ciccarello and Dransfeld[26] have pointed out that due to the finite lifetimes of the thermal phonons the resulting quantum mechanical uncertainty allows non co-linear longitudinal phonons to be involved in three-phonon processes. In fact they find that the interaction solid angle for longitudinal phonons is very nearly the same as for transverse phonons for all τ, as long as $\omega\tau > 1$. Thus they expect a T^4 dependence at all temperatures. They measured a T^4 dependence at 3 Gc/sec in Al_2O_3 for longitudinal waves as evidence for a strong three-phonon interaction for longitudinal waves. They also obtained for MgO a $T^{3.7}$ behavior for compressional waves and $T^{3.3}$ for transverse waves.

Woodruff and Ehrenreich[28] approached the theory of phonon-phonon scattering from the linearized Boltzmann equation and obtained results using approximations which are valid only in the region $\omega\tau << 1$ (high temperatures, low frequencies). However they feel that their results are also valid for $\omega\tau > 1$ since their results reduce to the same dependence on ω and T as obtained by Landau and Rumer[27] in this range. They also

obtain good agreement with the quartz data at 1 Gc/sec of Bommel and Dransfeld[18] over the entire range of measurements covering both $\omega\tau > 1$ and $\omega\tau < 1$.

These theories can therefore qualitatively account for the flattening out of the slope for tourmaline and for the T^4 dependence of quartz above 35°K. However they fail to account for the T^7 behavior in quartz and tourmaline observed in our measurements at lower temperatures and the T^9 behavior seen by de Klerk[25] in Al_2O_3 at 1 Gs/sec.

At 35°K the quantitative agreement of our quartz measurements with the Landau and Rumer theory is reasonable. Klemens[29] has given the results of this theory in the form,

$$\frac{1}{\ell_f} = 60\,\gamma^2 \left(\frac{KT}{Mv^2_{ave}}\right)\left(\frac{T}{\theta_D}\right)\frac{\omega}{v} \qquad (1)$$

where:

ℓ_f = mean free path of the acoustic phonon

γ = Grueneisen constant

K = Boltzmann constant = 1.38×10^{-16} erg/deg Kelvin

T = Temperature in degrees Kelvin

M = average atomic mass of crystal

v_{ave} = average sound velocity

θ_D = Debye temperature

v = sound velocity of acoustic wave

ω = angular frequency of acoustic wave

The reciprocal mean free path $1/\ell_f$ represents the fractional number of phonon interactions per cm. i. e.

$$\frac{1}{\ell_f} = \frac{dN/d\ell}{N} \cdot \tag{2}$$

Integrating over the phonon path length, L, we get

$$\int_{N_o}^{N} \frac{dN}{N} = \frac{1}{\ell_f} \int_0^L d\ell$$

$$\ell n \ \frac{N}{N_o} = \frac{L}{\ell_f}$$

The attenuation in db/cm is defined as

$$\alpha = \frac{1}{L} \ 10 \ \log_{10} \left(\frac{N_o}{N}\right) = \frac{10}{L} \ (.434) \ \ell n \ \left(\frac{N_o}{N}\right)$$

$$\alpha = -4.34 \ (1/\ell_f)$$

The average atomic mass of quartz (SiO_2) is M = 20 x 1.6 x 10^{-24} gm = 3.2 x 10^{-23} gm. The average sound velocity in α quartz is given by Anderson[23], v_{ave} = 6.05 x 10^5 cm/sec and the Debye temperature θ_D = 585°K. The Grueneisen constant is obtained from the formula[30].

$$\gamma = \frac{\beta V}{\kappa C_v} \tag{4}$$

where:

β = coefficient of cubical expansion

V = molar volume

C_v = molar heat capacity

κ = compressibility = reciprocal of bulk modulus

Values for these constants at room temperature for quartz[23,31] are $\beta = 5.1 \times 10^{-5}$, $V = 22.6$ cm^3/mole, $C_v = 6.18 \times 10^8$ erg/mole, $\kappa = 2.65 \times 10^{-12}$ cm^2/dyne. Thus $\gamma = 0.7$. The assumption is made here that the Grueneisen theory is exact and therefore is independent of the temperature, although this is not strictly true[30]. We note here that Woodruff and Ehrenreich[28] treated γ as an adjustable parameter in fitting their theory to the quartz data of Bommel and Dransfeld[18]. Their fits lay between values of $\gamma = 0.45$ to $\gamma = 0.87$.

The attenuation for quartz at 9.3 Gc/sec is thus predicted as

$$\alpha = 1.27 \times 10^{-6}\ T^4 \text{ db/cm} \tag{5}$$

At $T = 35^\circ$K this yields $\alpha = 1.90$ db/cm. Our measured value from Figure 8 at 35°K is 7.2 db/cm.

The difference is actually well within the uncertainty in the data used in deriving (5) since, e.g. Lord and Morrow[24] have values of

$\theta_D = 254^\circ K$ (instead of $585^\circ K$) and $C_v = 4.45 \times 10^8$ erg/mole (instead of 6.18×10^8 erg/mole). Using these values would give $\alpha = 57.4$ db/cm at $35^\circ K$.

Thus the attenuations observed in our experiments are certainly within the order of magnitude expected for three phonon processes. However, as pointed out above, the T^7 behavior is not accounted for. Klemens [29] discussed the contribution to the attenuation made by four phonon processes. He showed that

$$\frac{1}{\ell_f}(\mathrm{IV}) = \frac{10^{-11} T^4}{\ell_f(\mathrm{III})} \tag{6}$$

where $\ell_f(\mathrm{IV})$ is the mean free path of an acoustic phonon ending in a four phonon interaction and $\ell_f(\mathrm{III})$ is the mean free path for a three phonon process given by eq. (1). This would thus give a T^8 dependence, but with the 10^{-11} factor would be much too small to account for the observed attenuations.

Klemens [29] also suggested in a note added in proof than at lower temperatures the major contribution to the three phonon interactions come from thermal phonons with frequencies $\omega_{th} \simeq 6KT/\hbar$ rather than $\omega_{th} \simeq 4KT/\hbar$ as was the case in deriving eq. (1). Klemens concluded that this would yield a T^9 behavior at low temperatures, consistent with de Klerk's [25] observation with Al_2O_3. Our T^7 behavior could be the intermediate region between this T^9 dependence and the T^4 dependence at higher temperatures. An interpretation along these lines is being examined in greater detail.

The flattening of the attenuation in our tourmaline measurements would seem to imply that $\omega\tau < 1$ in the region above about $10^{\circ}K$ but a verification of this would depende on thermal conductivity measurements on tourmaline which as far as we know are not presently available.

Maris[32], as well as Ciccarello and Dransfeld[26] took into consideration the quantum mechanical uncertainty which results in a relaxation of the conservation of energy and momentum conditions for three phonon processes. However, he also took into account the dispersion for thermal phonons, which was ignored by Ciccarello and Dransfeld[26]. He got the result that in the vicinity of $40^{\circ}K$ the dependence should go as T^4 but it should begin to fall off faster at lower temperatues, in qualitative agreement with our results. He derives an expression for the attenuation

$$\frac{1}{\ell_f} = \frac{\pi^2 \hbar\, \omega\, \bar{F}^2}{60\rho^3 v^{10}} \left(\frac{KT}{\hbar}\right)^4 \left\{ \frac{\pi}{2} - \tan^{-1}\left[0.32\, \omega\tau \left(\frac{KTL}{\hbar v}\right)^2 \right] \right\}$$

where:

ρ = density of crystal

$\bar{F}_2$ = an average of third order elastic constants

L = average lattice spacing

τ = mean lifetime of thermal phonons

$\hbar$ = Planck's constant divided by 2π

Values of attenuation calculated from the expression yield 3.52, 0.98, 0.091, and 1.57×10^{-3} db/cm at 40°, 30°, 20°, and $10^{\circ}K$ respectively. These values are generally lower than our measured values. Also the fall off at lower temperatures is not as fast as the T^7 which we measure.

C. Crystal Preparation for Electron-Phonon Interaction Studies

1. Indium Antimonide

During the course of the program four separate crystals of InSb were obtained from Cominco Products, Inc., Spokane, Washington. The specifications indicated by the supplier for these crystals are noted in Table III.

Table III

Manufacturer's specifications for InSb crystals

		A	B	C	D
Type		n	n	n	n
R_H (cm^3/coul)	78°K	7.3×10^4	$(7.4\text{-}10.0) \times 10^4$	$(1.8\text{-}3.1) \times 10^4$	4.5×10^4
	300°K	310	370	370	360
ρ (Ω cm)	78°K	0.127	(0.07-0.16)	(0.035-0.040)	0.09
	300°K	4.0×10^{-3}	5.0×10^{-3}	5.0×10^{-3}	5.0×10^{-3}
μ (cm^2/volt sec)	78°K	5.7×10^5	$>5.0 \times 10^5$	$>5.0 \times 10^5$	$>5.0 \times 10^5$
	300°K	7.7×10^4	7.4×10^4	7.4×10^4	7.2×10^4
N_e (cm^{-3})	78°K	8.6×10^{13}	$(6.3\text{-}8.4) \times 10^{13}$	$(2.0\text{-}3.5) \times 10^{14}$	1.4×10^{14}
	300°K	2.0×10^{16}	1.7×10^{16}	1.7×10^{16}	1.7×10^{16}

a. Crystal A

The resistivity and Hall coefficient of two samples cut from this crystal were measured at 300°K and 78°K. They agreed reasonably well

with the manufacturer's specifications (measured values: ρ = 0.18 - 0.22 and R_H = 1.11 - 1.15 x 10^5 at 78°K - yielding μ = (5.35 - 6.09) x 10^5 and N_e (5.44 - 5.62) x 10^{13}).

The orientation of the (111) axis of this crystal was determined to within $\pm$ 2° using a back reflection Laue x-ray diffraction camera. With an ultrasonic cutter the crystal was cut into two 5/8" lengths with the cuts parallel to the (111) planes. These lengths of crystal were then cut into cylindrical rods 3 mm in diameter and 5/8" long again with the ultrasonic cutter maintaining the $\pm$ 2° accuracy of alignment between the (111) axis and the rod axis. These rods were then mounted with sealing wax into 3.2 mm diameter holes in the centers of two inch diameter, 5/8" thick glass disks. These disks were then optically polished so as to polish the ends of the rods. Optical interferometer methods were used on the disks during the polishing operations to insure that the end faces of the rods were held within 6 seconds of parallelism which is equivalent to about 0.08 acoustic wavelengths in InSb.

The rods thus obtained from crystal A were tried for acoustic propagation of longitudinal waves at 9.3 Gc/sec by several transducer bonding methods. None of them were successful in obtaining any detectable acoustic propagation through the crystal. The basic equipment used to perform all of these tests is that described in Section B-1 and shown in Figure 1 and 2.

The first method attempted involved attaching the quartz transducer rod to the InSb by a method which had been found very successful

for ultrasonic propagation in bonding tests between two quartz rods (resulting in nearly lossless bonds). This consisted of pressing the two polished surfaces together without any bonding agent between the surfaces but with a ring of Epoxy cement around the joint as illustrated in Figure 10a. This failed in bonding quartz to InSb since the difference in contraction caused the InSb to break each time.

The second method involved an attempt to overcome this difficulty. As is shown in Figure 10b, a frame of titanium was constructed such that it was glued to the walls of two quartz transducers but not to the InSb. The frame was glued on while the quartz transducers were held onto the InSb under pressure. Titanium was chosen because its coefficient of expansion lies between that of quartz (in the x-direction) and InSb. Thus by adjusting the length of the titanium frame relative to the InSb and the quartz it is possible to match the total contractions of the frame and the rods. No transmission of ultrasonic waves through the InSb crystal was observed in this test. The receiver detected a whole series of reflected echoes from the quartz-InSb interface indicating that the microwave equipment was working properly. Two cavities were used for this test on both ends of the quartz-InSb-quartz assembly. The receiver detected no echoes from the InSb either in the transmitting cavity or the receiving cavity. Thus the sound was highly attenuated either in the bonds or in the InSb itself. The sensitivity of the system is such that this represents a minimum attenuation of 40 db in the InSb and/or bonds.

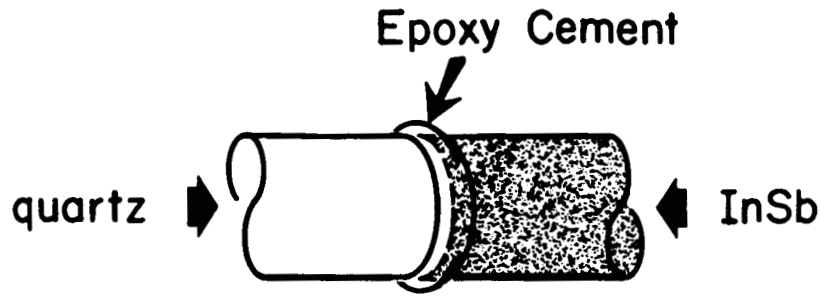

(a) Epoxy around joint but not between surfaces.

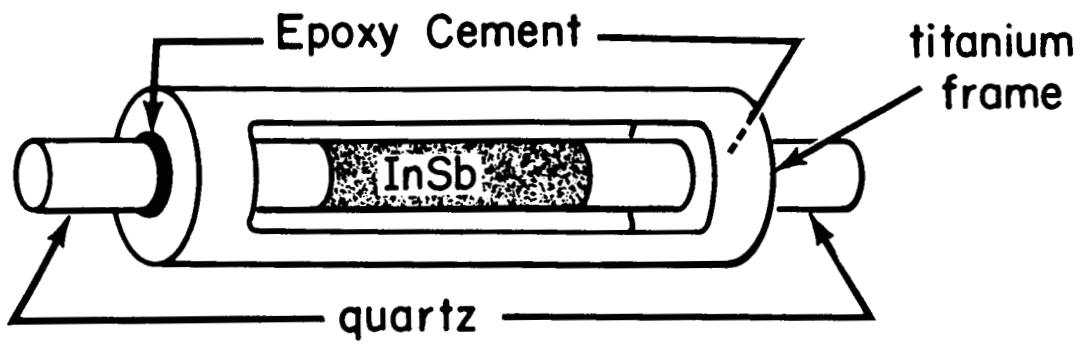

(b) Titanium frame holds rods together with no epoxy between the rod surfaces.

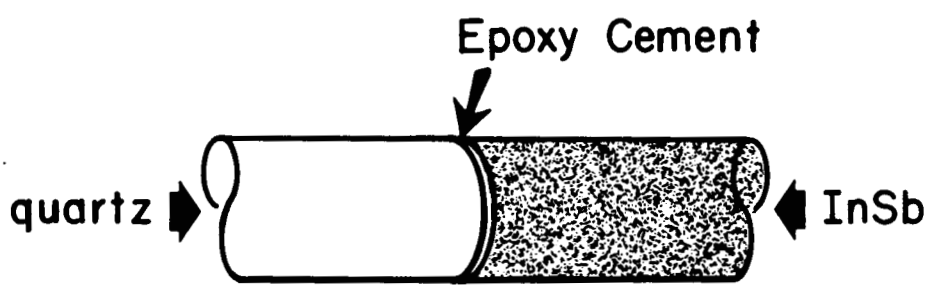

(c) Epoxy between the surfaces.

Fig. 10 TRANSDUCER BONDING METHODS

The third method consisted of straightforward bonding of InSb to quartz using a very thin film of Epoxy Cement between the surfaces as illustrated in Figure 10c. This technique for bonding involved pressing the quartz to the InSb with the interface under microscope observation. This insured elimination of all bubbles in the interface, thus improving the uniformity of the bond. This method has also proved successful for near lossless transmission of 9.3 Gc/sec phonons in bonding tests with two quartz rods. The same procedure was followed as in the second method and again no acoustic transmission was observed through InSb. The test was performed with an improved sensitivity such that a minimum of 55 db loss was observed in the InSb and/or the bond. If it were solely in the InSb this would represent an attenuation greater than 20 db/cm.

The fourth method amounted to simply inserting the InSb rod directly into the reentrant cavity, doing away with both quartz transducers. This attempt was based on the possibility that the piezoelectric coefficient of InSb would be large enough that it could act as its own transducer. This has the advantage of not involving any bonding problems. However, even though InSb lacks a center of inversion symmetry and is therefore expected to be piezoelectric, the binding is largely covalent and one expects the piezoelectric coefficient to be small. No transmission or reflection of acoustic waves was observed in this test.

b. Crystal B

The lack of a detectable transmitted signal in the second and third methods led us to suspect that perhaps the bonds were not at fault but that the signal was highly attenuated in the InSb. In order to be satisfied that we were not suffering seriously from off axis propagation[33] due to poor alignment of the (111) axis and the polished surface normal ($\pm$ 2°), we decided to make a better alignment. We therefore obtained another boat grown InSb crystal referred to as crystal B whose specifications are shown in Table III.

The method used to obtain better alignment involved the use of a precision x-ray spectrogoniometer shown in Figure 11. The x-rays from a Cu target were collimated onto the end of the InSb rod and the detector collimator was rotated to the correct position to pick up the first Bragg angle scattering of the copper K_α line from (111) planes in InSb. The goniometer holding the crystal was then rotated through its two degrees of freedom to maximize the x-ray counts in the geiger tube. This established the (111) axis as the bisecter of the source and detector collimator angle. Then the x-ray tube was removed from its location behind the source collimator and replaced by a light source. A photomultiplier tube was placed behind the detector collimator instead of the geiger tube. The crystal goniometer was again rotated through its two degrees of freedom until the light collected from specular reflection from the polished surface was a maximum. The difference between the two sets of readings on the crystal goniometer represented the angular deviation, δ, between the (111) axis and the surface normal.

Fig. 11 - X-ray spectrogoniometer with crystal in place.

The InSb rod with its glass disc was then removed from the spectrogoniometer and repolished to remove this angular difference. The entire process was again repeated until δ was less than 3 minutes of arc. Finally the reverse end of the rod was polished by the method described earlier using optical interference to make the reverse end parallel to the other end to within 6 seconds of arc.

Two tests of crystal B using the third transducer method described for crystal A were performed with equally negative results. In the second test a voltage pulse was applied across the InSb during the microwave pulse in the hope of amplifying any signal if it were present. In order to expect any amplification the electron drift velocity, v_D, produced by the applied voltage pulse must exceed the sonic velocity v_S in InSb. Since $v_S = 3.88 \times 10^5$ cm/sec in InSb[34], we attempted to apply a voltage pulse such that $v_D = 2v_S = 7.76 \times 10^5$ cm/sec. To estimate the voltage required we need to know the mobility at 4°K. According to data presented by Hilsum and Rose Innes[35], the Hall coefficient changes very little from 73°K to 4°K and the conductivity goes down by a factor of 33. Thus the mobility should go down by the same factor and we would expect therefore a mobility of $\mu_e = 1.5 \times 10^4$ cm^2 (volt sec)$^{-1}$ at 4°K. Thus $E = v_o/\mu_e = 52$ volts/cm requiring about 45 volts across a sample 0.86 cm long. The resistivity would be 4.9 Ωcm yielding a resistance of 60Ω for the 3 mm dia rod. These values do not agree with the values which we obtained when we applied pulses to the crystal. With pulses below 10 volts there was a resistance of about 100,000Ω (which was not present in the range 77°K - 300°K). However,

above 10 volts this resistance broke down and dropped to 1 ohm such that up to 80 volts the resistance remained at this value. The leads had been soldered with pure Indium using ruby flux after cleaning the contact area with fine sandpaper.

Later, checks of the resistivity and Hall coefficient of two samples cut from crystal B were made at $78^{\circ}K$ and $300^{\circ}K$. The leads were soldered ultrasonically with pure Indium and no flux. The results showed a change of sign in R_H between $300^{\circ}K$ and $78^{\circ}K$ indicating that the crystal was actually p-type rather than n-type as specified by the manufacturer. (InSb is always intrinsically n-type at room temperature unless very heavily doped). The temperature variation of resistivity was also measured between $4^{\circ}K$ and $265^{\circ}K$, yielding exactly the type of variation expected of p-type material[35]. The results are shown in Figure 12. This accounted for the high resistance seen at $4.2^{\circ}K$.

The lack of observed acoustic propagation in the InSb crystal led us to suspect strong attenuation due to interactions with dislocations in the crystals. We examined a sample cut from crystal B for grown-in dislocations by chemically etching the material long enough to polish off any surface dislocations produced in polishing. This was done using a standard etchant solution[36], CP4A (3 parts 48% HF, 5 parts 68% HNO_3 and 3 parts glacial CH_3COOH) for 10 seconds. A density of grown-in dislocation etch pits of $10^6/cm^2$ was observed (Figure 13a).

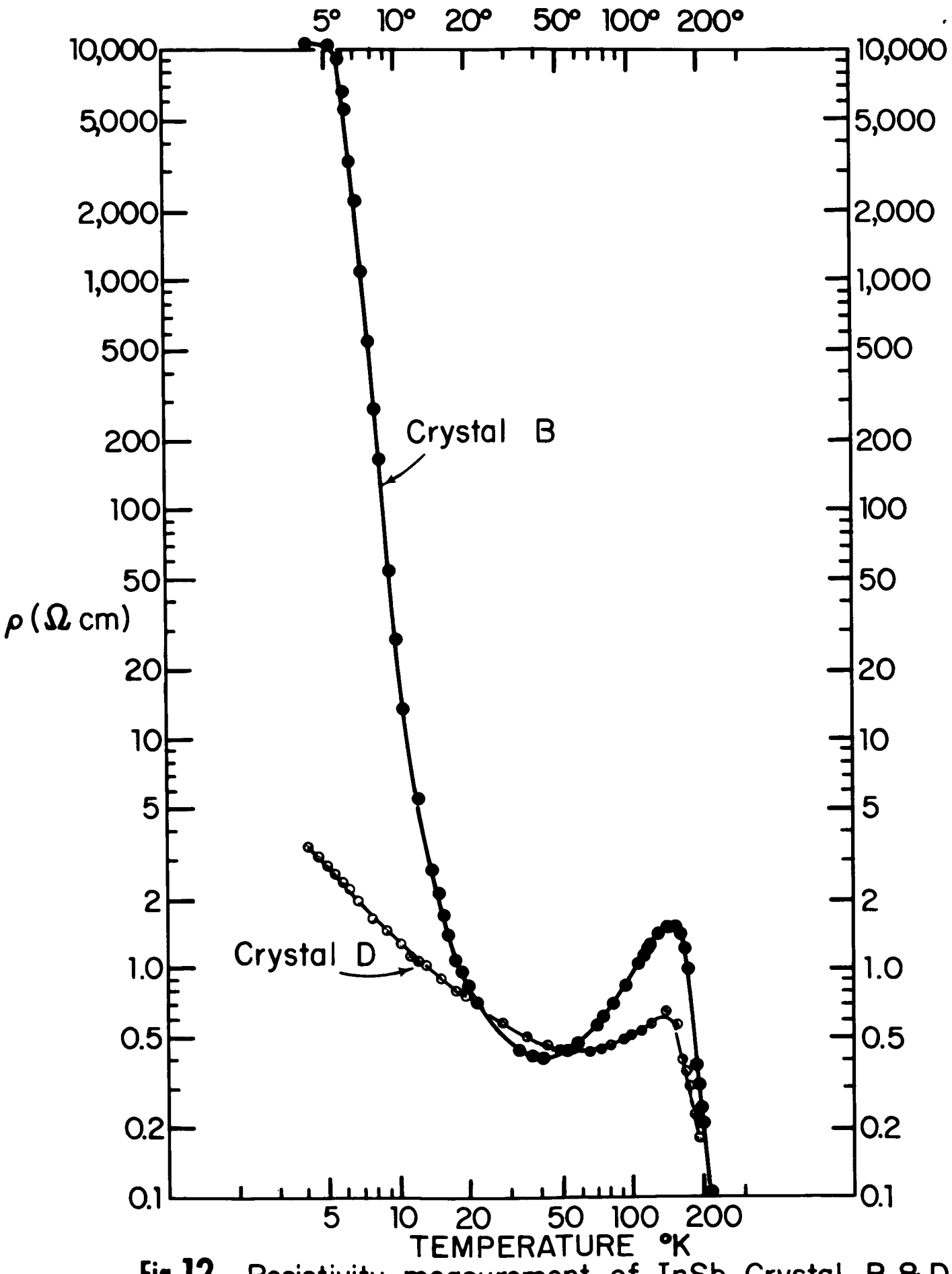

Fig.12 Resistivity measurement of InSb Crystal B & D

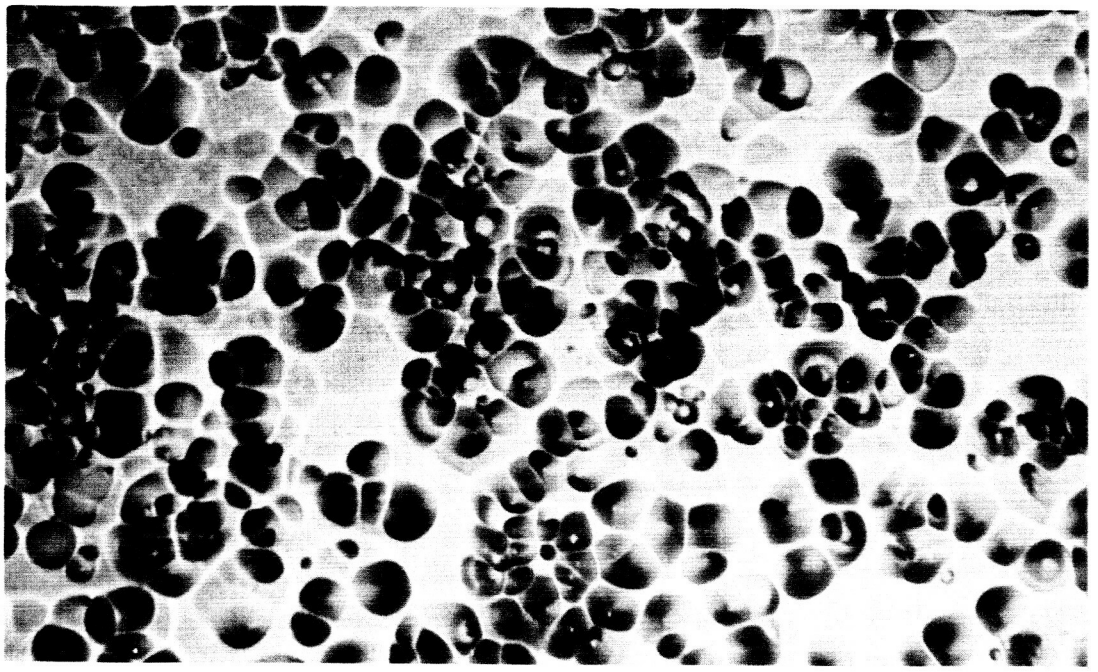

a. Crystal B, $10^6/cm^2$

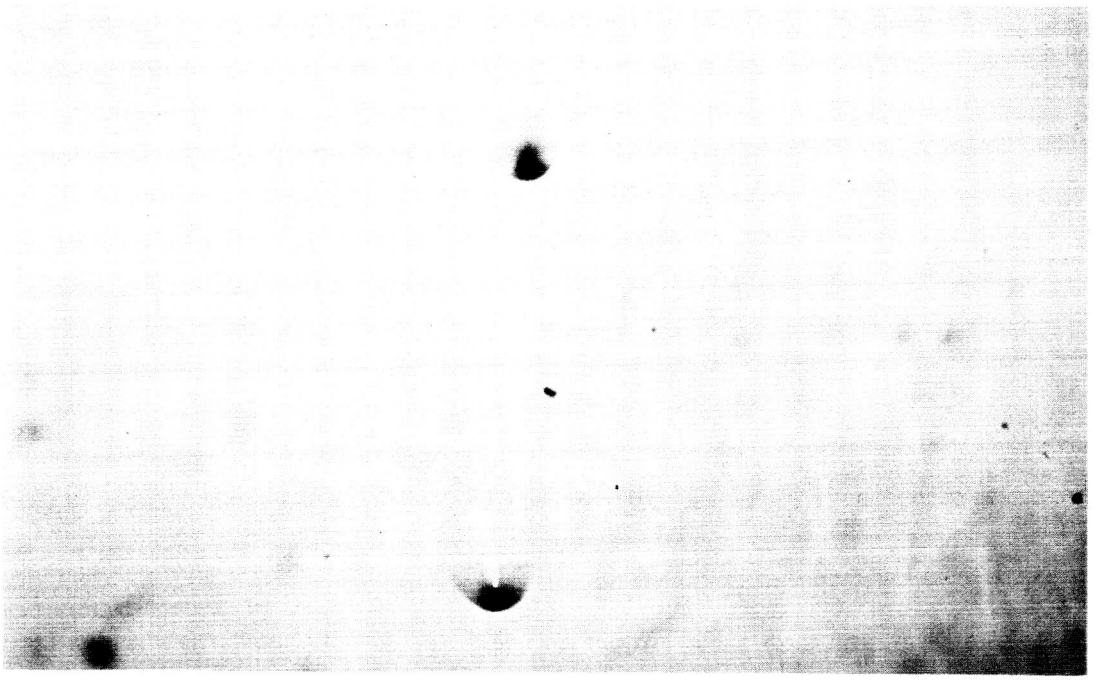

b. Crystal C, $45/cm^2$

Fig. 13 - Dislocation etch pits produced in InSb crystals using CP4A etchant for 10 secs. Magnification 625X.

c. Crystal C

Although it is possible to zone refine a boat-grown crystal to a higher purity than a pulled crystal, the boat-grown crystal tends to have a much higher dislocation density. It was therefore decided to obtain a crystal which was grown by the Czochraliski pulling method. This is crystal C listed in Table III. The same etchant was used for 10 seconds on crystal C as on crystal B and the photo of some of the resultant etch pits is shown in Figure 13b. The density measured was $45/cm^2$. If the high attenuation in Crystal B was due to the high dislocation density, then this crystal should be much better. Considerable unexpected difficulties were experienced in the cutting, aligning, and polishing of crystal C. In the ultrasonic cutting, it was very difficult to obtain a complete rod without breaking during the cutting process. This difficulty was not experienced at all with crystal B although it had been experienced to some extent with crystal A. Finally two rods were obtained. However, during the coarse polishing the rods seemed to develop small triangular chips in the surface. The triangular chips were characteristic of cleavage along three (110) surfaces, each one making an angle of 35^o with the (111) polished surface. This is not surprising since (110) planes are known cleavage planes in InSb. During the fine polishing the surface became concave. This was observed when checking the surface for flatness with an optical flat. About 3 or 4 interference rings were observed on the InSb surface. All of this behavior, which was not experienced in crystal B seemed to indicate that crystal C was considerably softer than crystal B.

Slower polishing speeds were tried with no significant improvement in the polishing characteristics. A soft lead glass obtained from Unertyl Optical Co. was tried with success in conjunction with slower polishing speeds. Finally a crystal 3.17 mm long was obtained having the surfaces flat to 500 Å and parallel to 20 seconds of arc. This figure for the parallelism represents about 0.6 acoustic wavelengths and therefore we would expect rather large interference effects.

Finally 9.3 Gc/sec phonons were observed to propagate in this crystal. The results will be discussed in Section D. However, the crystal was too short to effectively attach current leads to the ends to test the interaction of the phonons with conduction electrons. It must be remembered that the leads cannot be attached to the end faces of the crystal since these surfaces must be kept intact for acoustic transmission and reflection. Thus they have to be attached near the ends on the walls of the crystal. On such a short crystal the distance between leads would thus be too short compared to the diameter of the crystal.

d. Crystal D

A fourth InSb crystal was purchased, again Czochralski grown, but larger than crystal C so that rods long enough to attach current leads could be obtained. The resistivity for this crystal was also measured between $4.2^{o}K$ and $272^{o}K$ and although the results were not

in good agreement with the manufacturer's specifications they were, however, characteristic of n-type material[35]. The resistivity measurements are shown in Figure 12.

With the previous crystals, the x-ray spectrogoniometer (Fig. 11) had been used only for the final alignment of the crystals for polishing while the Laue diffraction camera had been used for the initial alignment for cutting. With crystal D the x-ray spectrogoniometer was used also for the initial alignment. This provided better alignment of the (111) axis with the rod axis. ($\pm$ 15' rather than $\pm$ 2°).

Due to chipping of the crystal before cutting into rods, the resulting rods were not quite the length planned. As it turned out after the polishing, the rods were of such a length (0.81 cm) that the acoustic transit time in the rods was nearly identical to the acoustic transit time in the quartz transducer rods which we had on hand. This condition of course makes it impossible to time separate acoustic echoes characteristic of transit through the InSb from those which traverse the quartz only. A number of solutions to this dilemma were possible but were precluded by the lack of time before the end of the contract. Longer quartz crystals could of course be used but the delivery time for these is too long. One of the rods could be cut shorter and polished but the polishing time would also preclude this solution. It was decided therefore to attach the polished rod to a quartz transducer and use it anyway. Leads were attached to the rod to look for changes in the echo amplitude with changes in current.

The current pulses were produced by a Hewlett Packard 212A pulse generator synchronised with the microwave system. In order to pump energy from the current pulse into the acoustic wave by way of the electron-phonon interaction it is necessary that the electron drift velocity exceed the sonic velocity. The timing of the pulse must also be adjusted such that it is on during the transit of the acoustic echo in one direction and off while the echo returns. We calculated the drift velocity, v_D, in the crystal from:

$$v_D = \mu E = R_H \sigma V/\ell = R_H \frac{\ell}{RA} \frac{IR}{\ell}$$

$$v_D = R_H I/A \qquad (7)$$

where:

I = current through the crystal

μ = electron mobility

E = electric field

V = voltage across the crystal

ℓ = length of crystal between the leads

σ = conductivity

R = resistance

A = cross sectional area

R_H = Hall coefficient

The Hall coefficient is essentially the reciprocal of the impurity concentration with a value of $R_H = 4.5 \times 10^4$ cm^3/coul for crystal D. Thus from eq (7) a current of 1.2 amps is necessary to obtain a drift velocity of twice the sonic velocity (3.88×10^5 cm/sec) of a longitudinal wave in the (111) direction of InSb. Such a pulse was applied and the results will be discussed in section D.

2. Other Semiconductors

Besides the InSb crystals obtained and tested during this program two other semiconductors were purchased from Cominco Products, Inc. These were GaAs and InAs. The manufacturer's specifications for the GaAs at 78°K were: $\rho = 0.28\Omega$cm, $\mu = 7.1 \times 10^3$ cm^2 (v-sec)$^{-1}$ and $N_e = 3.1 \times 10^{15}$ cm^{-3}. The data for InAs were $\rho = 0.007\Omega$cm, $\mu = 3.3 \times 10^4$ cm^2 (v-sec)$^{-1}$, and $N_e = 2.7 \times 10^{16}$ cm^{-3}.

These crystals were aligned using the x-ray spectrogoniometer as with InSb and were cut into rods. During polishing of the InAs, difficulties similar to those experienced with InSb crystal C were encountered. Once the problem had been solved as discussed above with InSb crystal C, time did not permit repolishing and testing of the InAs crystal with the improved method. The same is true for the GaAs crystal. Hickernell[37], in his extensive analysis of the electro-acoustic properties of III-V compounds, has pointed out that GaAs should be useful as an acoustic amplifier in the region above 1 Gc/sec.

D. Acoustic Propagation in InSb

As was pointed out in Section C, there was no observable propagation of 9.3 Gc/sec acoustic waves in InSb crystals A and B. Both of these crystals were boat grown with high disloation densities. The x-ray alignment of crystal A was good only to $\pm 2^{o}$ whereas crystal B was good to $\pm 3'$. Moreover, as it turned out, crystal B was p-type while crystal A was n-type.

With a 2^{o} misorientation, the energy flux would propagate at an angle[31] of $1.32 \times 2^{o} = 2.64^{o}$. This would result in approximately 30% loss of acoustic energy due to collision with the side wall before the first reflection. This could be a partial cause of high attenuation in crystal A. The p-type carriers (holes) in crystal B should not necessarily be a source of high attenuation. Crystal C which was n-type and oriented to within $\pm 6'$ with the (111) axis exhibited a very low attenuation. This crystal had a very low dislocation density. Thus it is concluded that the high dislocation density in crystals A and B was responsible for the high acoustic attenuation.

1. Temperature effects with Crystal C

The temperature dependence of 9.3 Gc/sec acoustic attenuation was studied with crystal C. A rod cut from this crystal and polished as discussed in section C-1-c, was attached to quartz rod #6 with

clear epoxy as discussed in section C-1-a for the third bonding method. This assembly is shown inserted in position in the cavity in Figure 3b.

A series of echoes was observed at 4.2°K which could be well identified with the number of passages through the quartz and the InSb rods. These echoes are shown in Figure 14 at the top. Each echo is labeled to identify the number of round trips through each crystal. For example, echo (0-1) represents the first reflection back from the quartz-InSb interface, (1-1) is the echo which traversed both the quartz and the InSb once. Echo (2-1) represents two round trips through InSb and one through quartz. It is evident from the size of echo (1-3), e.g. that the attenuation is very low and in fact is masked by interference effects. The identification of these echoes can be seen from Table IV which shows the expected timing of each echo based on the known acoustic transit time through the quartz and InSb rods. The table shows also the measured timing of the pulses of three different days' runs illustrating the complete unambiguity in identification.

The startling effect observed in these measurements is the <u>increase</u> in amplitude of some of the echoes as the temperature was increased. The lower photo in Figure 14 shows the echo pattern obtained after allowing the temperature to rise slowly to 12.1°K. (At this temperature the attenuation in quartz is still negligibly small as seen from Fig. 9.) This effect is particularly notable in echoes 2-5, 2-6, 2-7, and 3-8, although it is evident as well in echoes 2-1, 1-2, 2-2, 1-3, 2-3, 1-4,

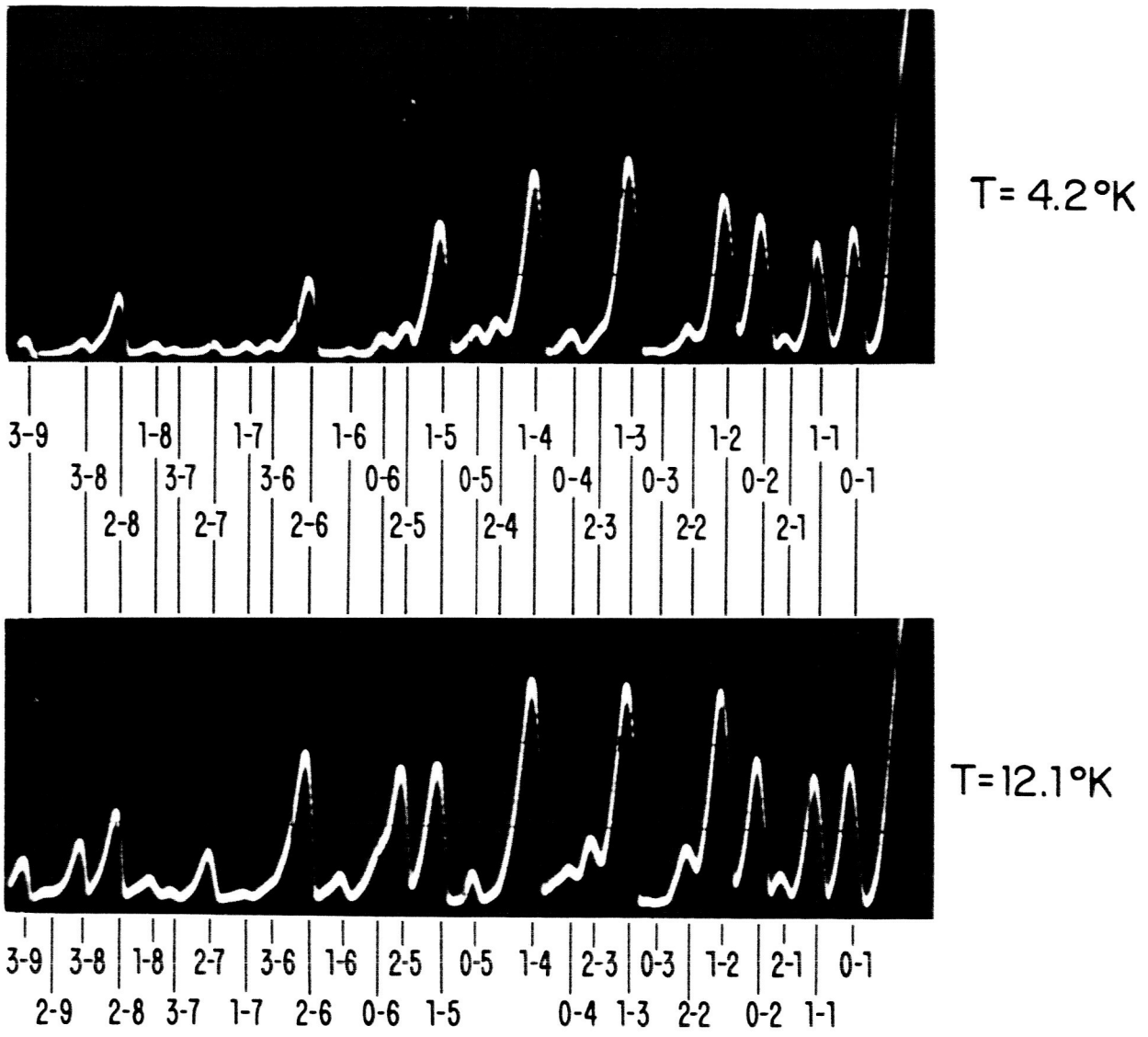

Figure 14 - Comparison at two different temperatures of acoustic echoes in InSb rod (from crystal C) bonded to a quartz transducer rod. Quartz rod 1.2 cm long, x-cut. InSb rod 0.32 cm long, (111)-cut. The symbols on the lines pointing to the echoes denote the number of round trips through InSb and through quartz. e.g., 0-1 represents one round trip through quartz only. Note the large increase in amplitude in echoes 2-5, 2-6, 2-7, 3-8 with increase in temperature.

Table IV

Expected and measured timing in μsecs. of acoustic echoes in quartz (1.27 cm long) bonded to InSb (0.32 cm long)

InSb round trips		quartz round trips 1	2	3	4	5	6	7	8	9	10	11
0	Calc.	4.5	9.0	13.5	18.0	22.5	27.0	31.5	36.0	40.5	45.0	49.5
	2nd run	4.6	9.1	13.5	18.0							
	4th	4.5	9.0	13.5	17.9							
	5th	4.6	9.1		18.1	22.6	27.1					
1	Calc.	6.2	10.7	15.2	19.7	24.2	28.7	33.2	37.7	42.2	46.7	51.2
	2nd run	6.3	10.8	15.3	19.7	24.2	28.7	33.3	37.7			
	4th	6.3	10.7	15.1	19.6	24.1	28.6					
	5th	6.3	10.8	15.3	19.7	24.3	28.5	33.3	37.5		46.6	
2	Calc.	7.9	12.4	16.9	21.4	25.9	30.4	34.9	39.4	43.9	48.4	52.9
	2nd run	8.0	12.5	17.0	21.4	26.0	30.5	35.0	39.4	44.0		
	4th	8.0	12.5	16.9	21.5	26.0	30.3	34.9	39.3	43.8		
	5th	8.0	12.6	17.0	21.6	25.8	30.5	34.9	39.3	43.8	48.5	
3	Calc.	9.6	14.1	18.6	23.1	27.6	32.1	36.6	41.1	45.6	50.1	54.6
	2nd run					27.7	32.2	36.7	41.2	45.6		
	4th								41.1	45.5		
	5th						32.4	36.8	41.0	45.5	50.3	54.8
4	Calc.	11.3	15.8	20.3	24.8	29.3	33.8	38.3	42.8	47.3	51.8	56.3
	2nd run								42.9	47.4		
	4th											
	5th											56.5
5	Calc.	13.0	17.5	22.0	26.5	31.0	35.5	40.0	44.5	49.0	53.5	58.0

2-8, and 3-9. A similar change is observed with increase in temperature on another day's run as seen in Figure 15. Here one can see the progressive increase in size of echoes 1-2, 1-3, 1-4, 2-5, 2-6, 2-7 and 2-8.

In comparing Figs. 14 and 15 we see that, although the increase with temperature for some echoes is qualitatively reproducible from one day's run to another (several other days' runs not illustrated here show the same effect as well), the echo patterns do not reproduce in detail after thermal cycling. A similar irreproducibility after thermal cycling has already been noted in the echo patterns of quartz alone (Fig. 5). It is likely that again, these day to day changes are due to springing in the quartz transducer, changing the parallelism of the quartz faces.

It is possible to make some generalization about the increase in amplitude with temperature observed for some of the echoes. The increase was observed only for echoes which traversed the InSb, not for those which traversed the quartz only. The largest increases occurred for echoes representing two or three passes through the InSb although all such echoes did not show increases. Typical data for the run illustrated by the oscilloscope pictures of Figure 15 is shown in Figure 16. This data illustrates the above generalization.

It is tempting, on the basis of these generalizations, to ascribe these increases in amplitude to a decrease in attenuation with increase in temperature for InSb. Although some of the increases are very large (~14 db), it is not possible to identify these increases with a

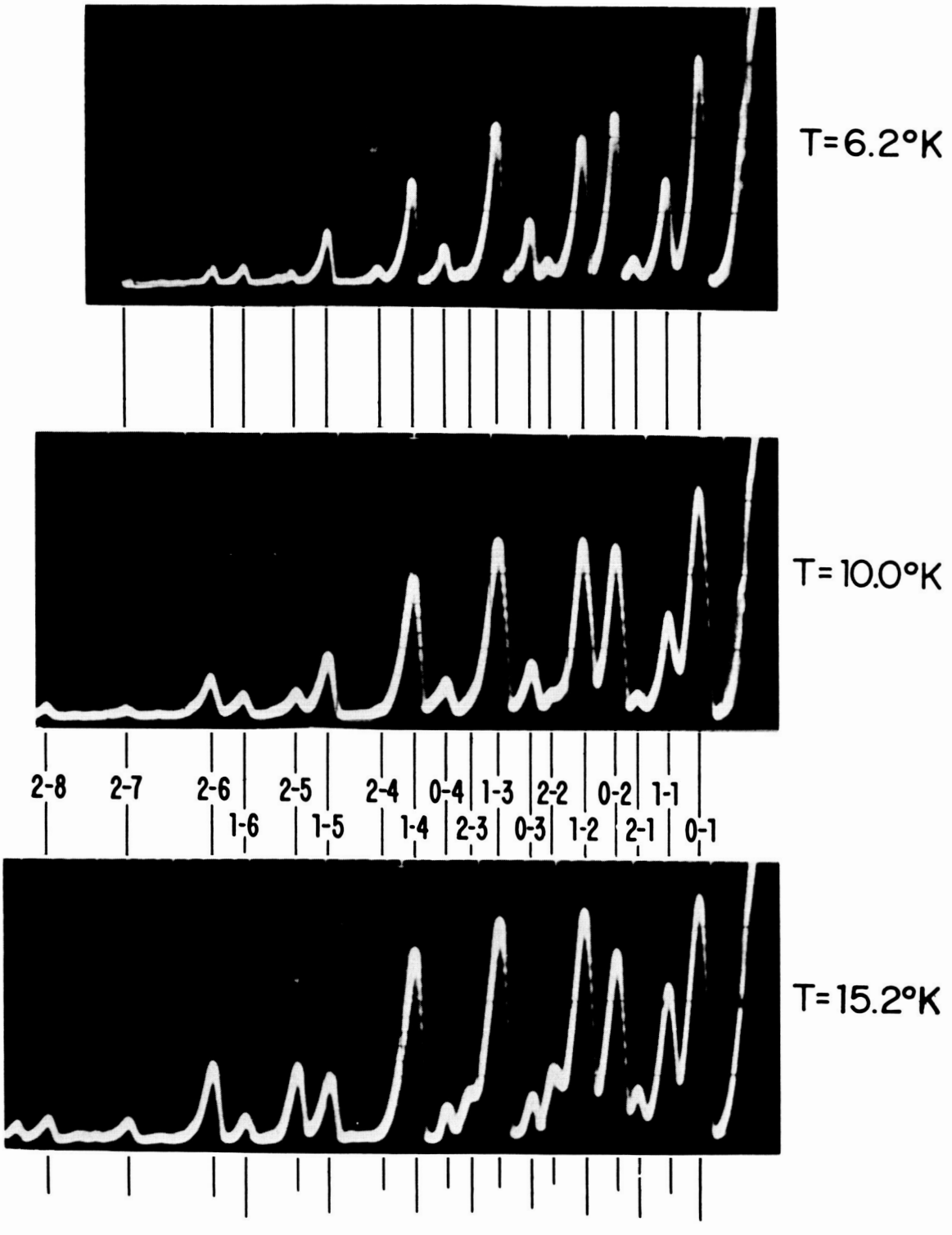

Figure 15 - Comparison of 9.3 Gc/sec acoustic echoes in the InSb and quartz (same as Figure 14) at 6.2°K, 10.0°K and 15.2°K. These data were taken on a different day from the data in Figure 14. Differences in relative amplitudes between the two runs are evident but the large increase of amplitude with temperature for echoes 2-5 and 2-6 is still evident. Increases in other echoes such as 1-1, 1-2, 1-3, 1-4 and 2-7 are also seen.

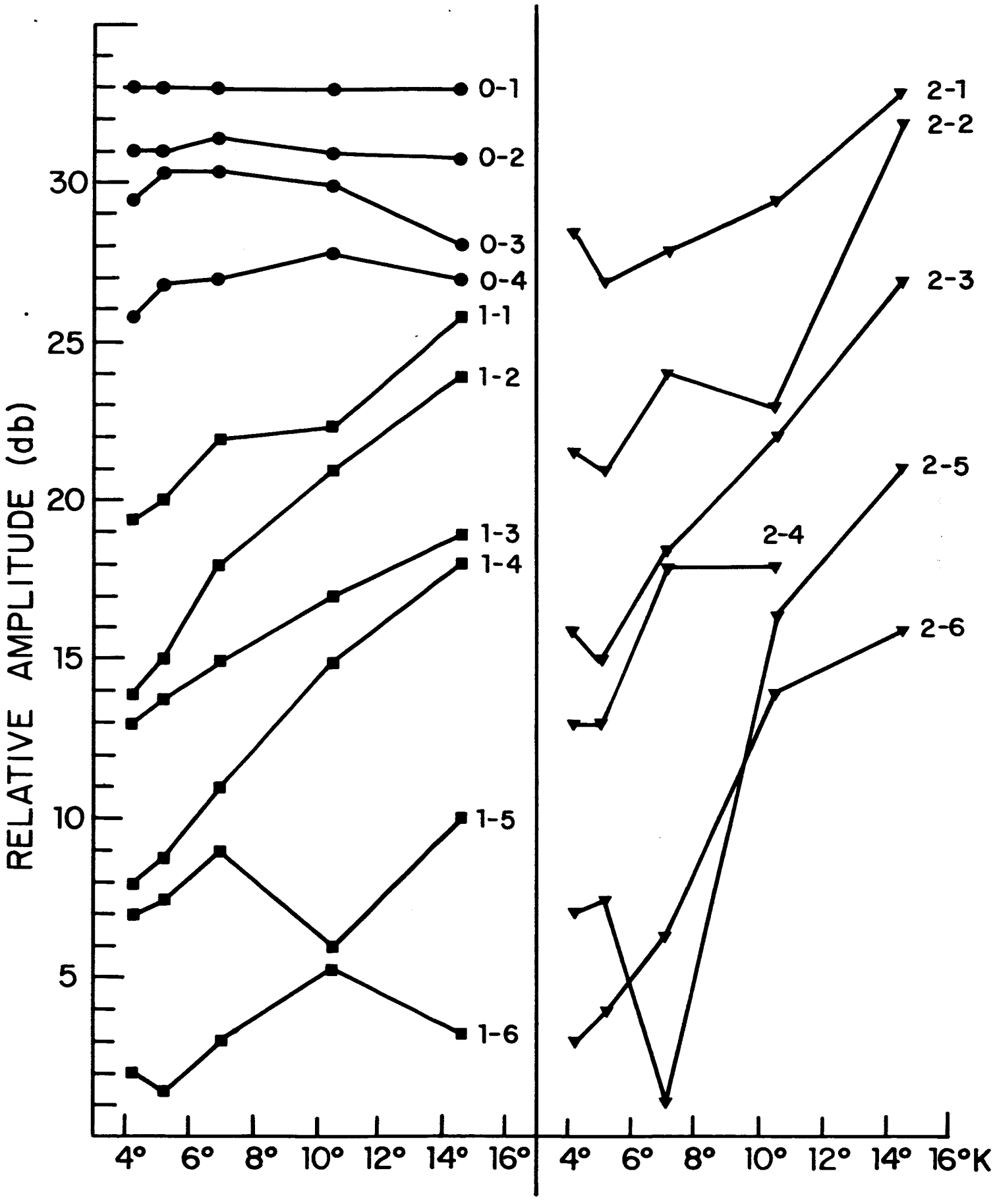

Fig. 16 Variation of various echo amplitudes in the InSb + quartz assembly. The correct relative amplitude between echoes is not shown here for the sake of clarity in presentation.

quantitative measure of attenuation decrease in InSb. The reason for this is of course the strong interference effects which are not necessarily constant with temperature. Although the interference effects observed in quartz alone as discussed in Section B-3-b were completely independent of temperature in this range, this might not be so with InSb or with the bond between the crystals. Thus it is possible that these increases are merely a manifestation of changes in the interference pattern. However, since there are no significant decreases, as well as increases, one must still consider the likelihood that these changes represent a real reduction of attenuation in InSb with increase in temperature. This would be in direct contradiction to data presented recently by Nill and McWhorter[38] for 9 Gc/sec attenuation in InSb. They saw a very fast increase in attenuation with temperature.

In order to establish the answer to this question further experiments will have to be performed, using other InSb crystals with hopefully better alignment of end faces. Use of the evaporated thin film piezoelectric transducer technique described by de Klerk and Kelly[39] would help to remove many ambiguities due to the bond and the transducer.

2. Frequency effects with Crystal C

In addition to the temperature dependent amplitude changes discussed above, we observed a frequency shift in the echoes traversing InSb. This shift displayed itself by requiring a slightly different

local oscillator frequency to maximize the echoes which traversed the InSb. This effect is illustrated in Figure 17 which shows in the top photo, the echo pattern obtained when the local oscillator is adjusted to maximize echo 1-1 and in the lower photo the pattern corresponding to maximizing echo 0-1 with the local oscillator. It is evident that all the echoes traversing quartz alone maximize with echo 0-1. These are identified in the lower photo. It is also evident that echoes traversing InSb tend to maximize with echo 1-1. This effect can be interpreted as a frequency shift in the acoustic wave as it travels through the InSb. The shift amounted to an increase of about 1-2 Mc/sec. Several attempts were made to see if twice the shift occurred with pulses corresponding to two trips through the InSb. The results of these attempts were not conclusive due to the large uncertainties involved in measuring the actual magnitude of such a small change of frequency (1 part in 10^4).

3. Preliminary tests with Crystal D

As discussed in Section C-1-d, InSb crystal D unfortunately ended up with a length exactly equal in transit time to the quartz transducers on hand. Thus the unambiguous time separation of echoes used with crystal C was not possible here. Therefore any echoes corresponding to traversal through InSb were not identifiable. One would still expect to see the temperature effects and the frequency effects discussed in connection with Crystal C to exhibit themselves in this case. The crystal was bonded with epoxy to quartz crystal #7 exactly as was done with crystal C.

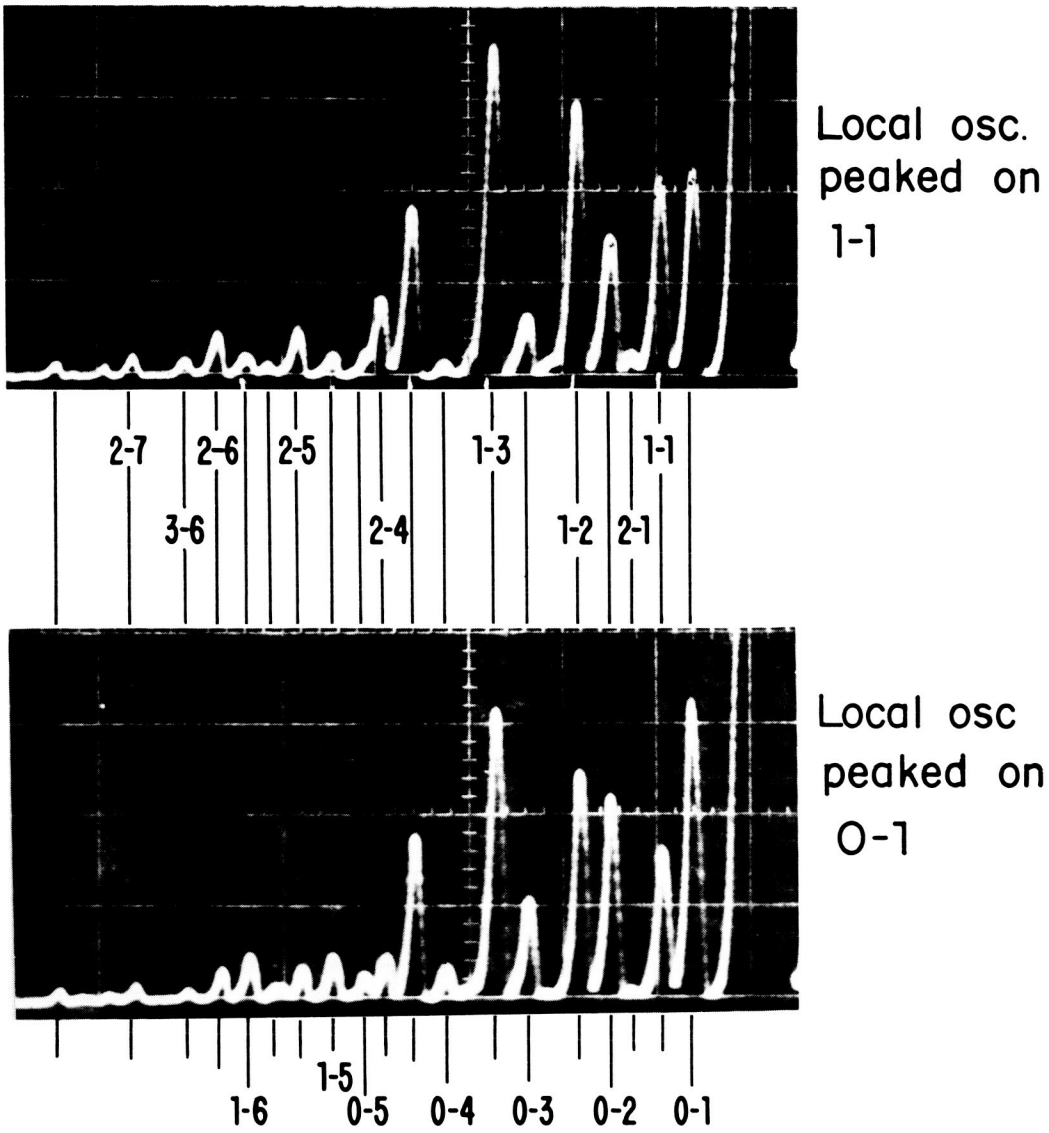

Figure 17 - Comparison of 9.3 Gc/sec acoustic echoes in the InSb and quartz (same as Figure 14) at 4.2°K, for two different tunings of the local oscillator. The echoes labeled in the top photo are those which became larger when the local oscillator was tuned to maximize echo 1-1. Those labeled on the lower photo maximized with echo 0-1. The top photo represents a frequency ~2 mc/sec higher than the lower photo.

The frequency shift effect seen with crystal C seems to show up to some extent here. Figure 18 shows the echo pattern obtained when the local oscillator is adjusted to maximize the third echo in the top photo and the fourth echo in the lower photo. There is apparently some change occurring here but it cannot be interpreted further due to the similarity of transit times. It does appear also that all the echoes beyond the 4th get larger when the local oscillator is peaked on the 4th echo.

An examination of the pulses in the temperature range from $4.2^{o}K$ to $21.7^{o}K$ revealed no significant change in the echo pattern in this temperature range until the attenuation in quartz became noticeable above $15^{o}K$. The magnitude of the effects seen for crystal C is such that similar effects should have been visible here if they existed. This could imply one of three possibilities:

1) The changes seen in crystal C were due to some peculiarity of the bond which did not exist in this case.
2) The attenuation in the InSb was very much higher here than for crystal C.
3) Some differences between the InSb in crystal C and crystal D caused a significant difference in the temperature variation observed with crystal C.

The first possibility does not seem to be a sufficient explanation since one would expect bond differences to show up as perhaps a different behavior from one bond to another but not to be very strong in one and non-existent in another. The second possibility

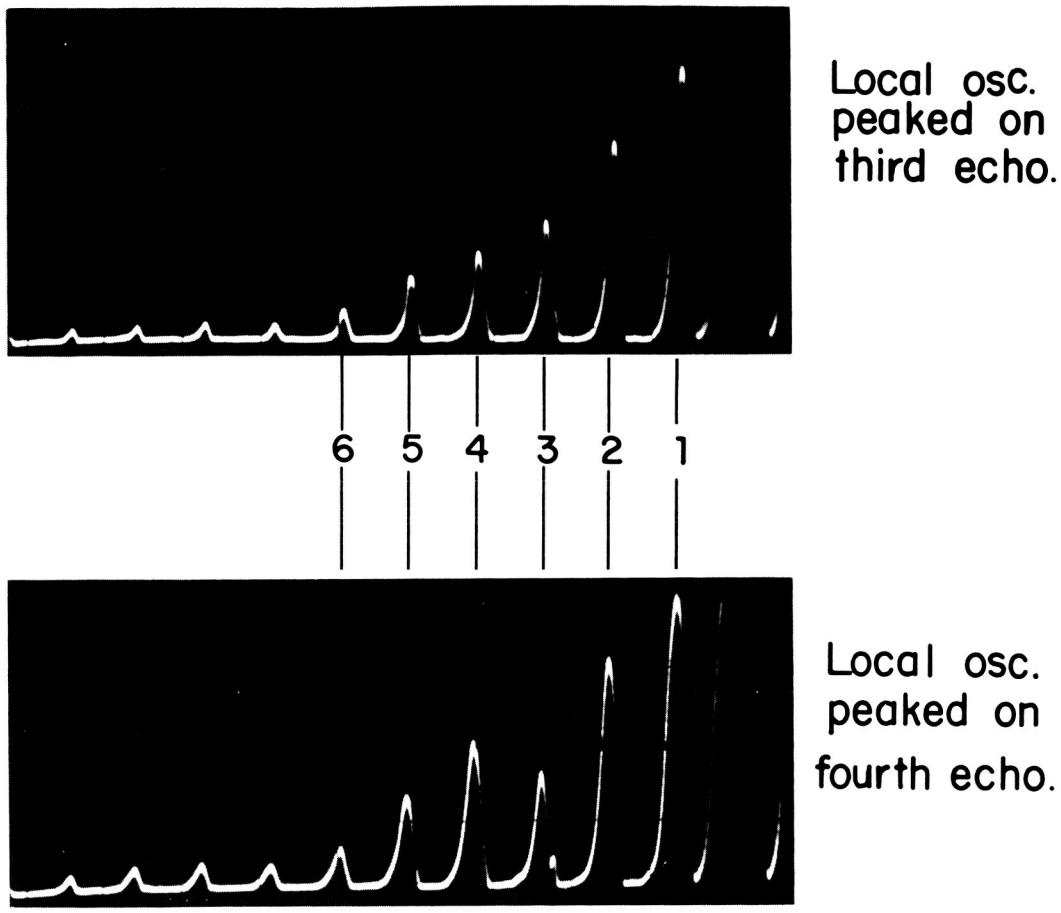

Figure 18 - Comparison of 9.3 Gc/sec acoustic echoes in InSb rod (from crystal D) bonded to a quartz transducer rod. Quartz rod 1.27 cm long, x-cut. InSb rod 0.81 cm long (111)-cut. Because of the identical acoustic transit times in the two rods, the echoes from InSb and quartz are superimposed. Note the sensitivity to tuning which had been observed also in Figure 17.

does not seem to be entirely true, since the frequency shift effects seen with Crystal C somehow seem to show through here also. This leaves us with the possibility of the third explanation. This will need to be examined in considerably more detail by measurements of all the electrical properties of the two crystals in question. Of course repeated measurements of the microwave acoustic echoes with better transducer conditions on several samples from the same crystal is desirable.

Finally, a check on the effect of adding a current pulse across the InSb crystal during the acoustic propagation was tried. The results of this attempt were somewhat inconclusive although the effect was definitely small. A current pulse 2.2 μsec long ranging from 0 to $\pm$ 1.2 amps (1.2 amps corresponds to moving the electrons at twice the sonic velocity) was used with the timing varied over a wide range. The 2.2 μsec duration corresponds to a one-way acoustic path length in the InSb crystal. Under no circumstance was a change greater than 1 db observable. There did however, appear to be repeatable changes which occurred as the current pulse was varied in time with respect to the echo pattern. The direction of the change appeared to reverse with change in local oscillator tuning. This seems to be connected with the frequency shift effect discussed earlier. The timing of the current pulse corresponding to these changes was not clearly coincident with the time of propagation of the acoustic wave through the InSb. At the present time the only conclusions that can be drawn about these tests are that any effect which may exist is small.

E. Summary and Conclusions

Measurements were made of attenuation of 9.3 Gc/sec acoustic waves in quartz and tourmaline crystals as a function of temperature. The acoustic waves were generated by piezoelectric excitation of the crystal surface in a reentrant microwave cavity. The measurements on quartz agreed well with the data of other investigators over the range of overlap and extended the dynamic range of the data considerably. A change in the power of the temperature dependence was observed with both quartz and tourmaline. The T^n variation for quartz extended from n = 7 at 15°K to n = 4 at 40°K while for tourmaline we measured n = 7.5 at 6°K and n = 0.8 at 95°K. It was concluded that qualitatively the quartz and tourmaline results were consistent with phonon-phonon scattering theories at the higher temperature end but that the high value of n at the lower temperatures was not adequately explained.

A large variability in acoustic echo patterns in quartz was observed after repeated thermal cycling. The temperature dependent part of the attenuation was, however, quite independent of this variability in the crystals. These effects were presumed to be due to changes in the stresses in the crystal, causing a change in the parallelism of the end faces.

Four high purity single crystals of InSb were obtained and prepared for electron-phonon interaction tests. The preparation involved orienting, cutting, final orienting and polishing of the crystals such that the final products were 3 mm diameter single crystal rods with end faces

polished flat and parallel to each other and normal to the (111) axis. The cutting and polishing characteristics of these crystals were not the same from one crystal to the other and considerable difficulty was encountered, particularly with the third crystal. These crystal rods were bonded to quartz rods used as transducers. Several bonding methods were tried, but the straightforward method of bonding with a thin film of epoxy was settled on.

No acoustic propagation was observed in rods cut from the first two crystals with or without a drift current of electrons in the crystal. This was interpreted as a high attenuation due to some source other than electron-phonon interaction, since a large electron-phonon interaction would produce an acoustic gain when the electron drift velocity exceeds the acoustic velocity. However phonons were propagated in a rod cut from the third crystal and exhibited a very low attenuation. The significant difference between this crystal and the other two was the dislocation density, which was very much smaller in the third crystal. It was concluded that dislocation scattering was responsible for the high attenuation in the first two crystals.

Two rather surprising effects were seen in phonon propagation in the third InSb crystal. One was an apparent decrease in attenuation with increase in temperature between $4.2^{\circ}K$ and $15^{\circ}K$. The other was a frequency shift of 1-2 Mc/sec in the phonons propagating through the InSb. The fourth crystal was prepared and examined for these effects, but due to

an unfortunate chipping of the crystal, the first test (the only one which time allowed during the course of the contract) was somewhat ambiguous in its results. The acoustic length of the crystal turned out to be identical to that of the quartz transducer. The tentative conclusion about the strange temperature variation is that it could be a peculiar bond effect but that a real effect in the crystal can by no means be ruled out. Further experimental investigation of this effect is certainly warranted. The frequency shift effect was seen consistently in the third crystal and appeared to be present also in the fourth crystal. The shift consisted of an increase in frequency and a more precise determination of its magnitude will be necessary.

No electric current pulse was applied in the tests of the third crystal since the rod was too short (0.32 cm) to effectively attach current leads near the ends. Such pulses were applied in the tests of the fourth crystal but no clear effect was seen. A very small effect seemed to exist but due to the ambiguity mentioned above it was not possible to interpret it sensibly.

A continued study of the above effects is recommended as well as an extension of the work to other semiconductors. In particular, crystals of GaAs and InAs have been oriented and cut for this purpose, but have not yet been polished and tested.

References

1. A. Z. Akcasu and R. K. Osborn, Damping Theory and its Application to Neutron Scattering by Anharmonic Crystals, Nuovo Cimento, 38 175 (1965).

2. E. H. Jacobsen, Experiments with Phonons at Microwave Frequencies, Quantum Electronics, Columbia Univ. Press, 469 (1960).

3. M. H. Seavey, Microwave Phonon Generation by Thin Magnetic Films, IEEE Trans. on Ultrasonic Engineering UE-10 49 (1963).

4. H. E. Bommel, Ultrasonic Attenuation in Superconducting and Normal-conducting Tin at Low Temperatures, Phys. Rev., 100, 758 (1955).

5. The Fermi Surface, edited by W. A. Harrison and M. B. Webb (John Wiley and Sons, Inc., New York, 1960).

6. N. Tepley, An Application of Microwave Frequency Ultrasonics to the Measurement of the Fermi Surface of Gallium, Ph.D. Thesis, Mass. Inst. of Technology (August, 1963).

7. E. I. Blount, Ultrasonic Attenuation by Electrons in Metals, Phys. Rev. 114, 418 (1959).

8. M. H. Cohen, M. J. Harrison, and W. A. Harrison, Magnetic Field Dependence of the Ultrasonic Attenuation in Metals, Phys. Rev., 117, 937 (1960).

9. A. P. Pippard, A. Proposal for Determining the Fermi Surface by Magneto-Acoustic Resonance, Phil. Mag., 2, 1147 (1957).

10. Gabriel Weinreich, Acoustodynamic Effects in Semiconductors, Phys. Rev., 104, 321 (1956).

11. A. R. Hutson, J. H. McFee, and D. L. White, Ultrasonic Amplification in CdS, Phys. Rev. Letters, 7, 237 (1961).

12. A. R. Hutson and D. L. White, Elastic Wave Propagation in Piezoelectric Semiconductors, J. Appl. Phys., 33, 40 (1962).

13. D. L. White, Amplification of Ultrasonic Waves in Piezoelectric Semiconductors, J. Appl. Phys., 33, 2547 (1962).

14. J. H. McFee, Ultrasonic Amplification and Non-Ohmic Behavior in CdS and ZnO, J. Appl. Phys., 34, 1548 (1963).

15. H. N. Spector, Amplification of Acoustic Waves Through Interaction with Conduction Electrons, Phys. Rev. 127, 1084 (1962).

16. J. R. A. Beale and M. Pomerantz, Acoustoelectric Effect of Microwave Phonons in GaAs., Phys. Rev. Letters, 13, 198 (1964).

17. M. Pomerantz, Propagation of Microwave Phonons in Germanium, IEE Trans. on Sonics and Ultrasonics, SU-11, 68 (1964).

18. H. E. Bommel and K. Dransfeld, Excitation and Attenuation of Hypersonic Waves in Quartz, Phys. Rev., 117, 1245 (1960).

19. M. H. Seavey, Jr. and W. J. Kearns, Microwave Absorption and Longitudinal Phono Generation by "Stripe" Domains in Permalloy Films (Ni-Fe). Appl. Phys. Letters 5, 23 (1964).

20. R. L. Powell and M. D. Bunch, The Thermal E.M.F. of Several Thermoelectric Alloys. Bull. Inst. Internat. Froid Annexe 1958-1, p. 129. Also - Cryogenic Engineering, R. B. Scott, p. 349 Van Nostrand (1959).

21. M. Pomerantz, Temperature Dependence of Microwave Phonon Attenuation, Phys. Rev., 139, A501 (1965).

22. R. Nava, R. Azrt, I. Ciccarello and K. Dransfeld, Hypersonic Absorption in Quartz at Temperatures Below 30°K, Phys. Rev., 134, A581 (1964).

23. O. L. Anderson, Determination and Some Uses of Isotropic Elastic Constants of Polycrystalline Aggregates using Single-Crystal Data, Physical Acoustics, edited by W. P. Mason, Vol. 3B, Chap. 2 (1965).

24. R. C. Lord and J. C. Morrow, Calculation of the Heat Capacity of α-Quartz and Vitreous Silica From Spectroscopic Data, J. Chem. Phys., 26, 230 (1957).

25. J. De Klerk, Behavior of Coherent Microwave Phonons at Low Temperatures in Al_2O_3 using Vapor-Deposited Thin-Film Piezoelectric Transducers, Phys. Rev., 139, A1635 (1965).

26. I. S. Ciccarello and K. Dransfeld, Ultrasonic Absorption at Microwave Frequencies and at Low Temperatures in MgO and Al_2O_3, Phys. Rev. 134, A1517 (1964).

27. L. Landau and G. Rumer, Sound Absorption in Solid Bodies, Phys. Zeits. der Sowjet Union, 11, 18 (1937).

28. T. O. Woodruff and H. Ehrenreich, Absorption of Sound in Insulators, Phys. Rev., 123, 1553 (1961).

29. P. J. Klemens, Effect of Thermal and Phonon processes on Ultrasonic Attenuation, Physical Acoustics, edited by W. P. Mason, Vol. 3B, Chap. 5 (1965).

30. M. Blackman, The Specific Heat of Solids, Handbuch der Physik, Vol. VIII/1 p. 380 (1955).

31. Handbook of Chemistry and Physics, Chemical Rubber Publishing Co. and American Institute of Physics Handbook, McGraw Hill Book Co.

32. Humphrey J. Maris, On the Mean Free Path of Low Energy Phonons in Single Crystal Quartz, Phil. Mag. 9, 901 (1964).

33. P. C. Waterman, Orientation Dependence of Elastic Waves in Single Crystals, Phys. Rev., 113, 1240 (1959).

34. L. H. De Vaux and F. A. Pizzarello, Elastic Constants of Indium Antimonide, Phys. Rev., 102, 85 (1956).

35. C. Hilsum and A. C. Rose-Innes, Semiconducting III-V Compounds, Pergamon Press (1961).

36. H. C. Gatos and M. C. Lavine, Chemical Behavior of Semiconductors: Etching Characteristics, Tech. Rep. No. 293, Mass. Inst. of Technology, Lincoln Laboratory (Jan. 1963).

37. F. S. Hickernell, The Electroacoustic Properties of III-V Compounds, Air Force Avionics Lab., Wright-Patterson Air Force Base, Technical Report AFAL-TR-65-136 (April 23, 1965).

38. K. W. Nill and A. L. McWhorter, Magnetoacoustic Effects at 9 Gc/sec in n-InSb, Bull. Am. Phys. Soc., 11, 259 (1966).

39. J. de Klerk and E. F. Kelly, Vapor-Deposited Thin-Film Piezoelectric Transducers, Rev. Sci. Inst., 36, 506 (1965).